Title

DTX3L ubiquitin ligase ubiquitinates single-stranded nucleic acids

Authors

Emily L. Dearlove[1,2†], Chatrin Chatrin[1,2,3†], Lori Buetow[1], Syed F. Ahmed[1], Tobias Schmidt[1], Martin Bushell[1,2], Brian O. Smith[4] and Danny T. Huang[1,2*]

Affiliations

[1]Cancer Research UK Scotland Institute, Garscube Estate, Switchback Road, Glasgow, G61 1BD, United Kingdom.

[2]School of Cancer Sciences, University of Glasgow, Glasgow, G61 1QH, United Kingdom.

[3]Present address: Sir William Dunn School of Pathology, University of Oxford, Oxford OX1 3RE, United Kingdom.

[4]School of Molecular Biosciences, University of Glasgow, Glasgow, G12 8QQ, United Kingdom.

[†]These authors contributed equally to this work.

[*]Correspondence: d.huang@crukscotlandinstitute.ac.uk

Abstract

Ubiquitination typically involves covalent linking of ubiquitin (Ub) to a lysine residue on a protein substrate. Recently, new facets of this process have emerged, including Ub modification of non-proteinaceous substrates like ADP-ribose by the DELTEX E3 ligase family. Here we show that the DELTEX family member DTX3L expands this non-proteinaceous substrate repertoire to include single-stranded DNA and RNA. Although the N-terminal region of DTX3L contains single-stranded nucleic acid binding domains and motifs, the minimal catalytically competent fragment comprises the C-terminal RING and DTC domains (RD). DTX3L-RD catalyses ubiquitination of the 3'-end of single-stranded DNA and RNA, as well as double-stranded DNA with a 3' overhang of two or more nucleotides. This modification is reversibly cleaved by deubiquitinases. NMR and biochemical analyses reveal that the DTC domain binds single-stranded DNA and facilitates the catalysis of Ub transfer from RING-bound E2-conjugated Ub. Our study unveils the direct ubiquitination of nucleic acids by DTX3L, laying the groundwork for understanding its functional implications.

INTRODUCTION

Ubiquitination—the covalent attachment of ubiquitin (Ub) to a substrate—is a versatile post-translational modification involved in the regulation of various cellular functions (*1*). The most widely studied examples of this modification involve conjugation of Ub to lysine residues in proteinaceous substrates. Non-lysine ubiquitination of protein substrates via serine (*2*) and threonine (*3*) residues has also been demonstrated. The modification of these residues produces an ester linkage in contrast to the canonical isopeptide amide bond that is observed in the ubiquitination of lysine residues (*4*). In recent years, non-proteinaceous ubiquitination substrates have emerged. These substrates include bacterial lipopolysaccharide which is ubiquitinated by RNF213 in the immune response to *Salmonella* (*5*), glucosaccharides which are ubiquitinated by HOIL-1 (*6*) and adenosine 5′-diphosphate (ADP)–ribose (ADPr) which is ubiquitinated by the Deltex family of ubiquitin ligases (E3s) (*7-9*). Collectively, these studies have uncovered that the diversity of substrates undergoing ubiquitination expands beyond that of proteinaceous substrates. Additionally, they highlight that this mechanism is not limited to one E3 ligase family.

The Deltex (DTX) E3 family is comprised of five RING E3s, DTX1, DTX2, DTX3, DTX3L and DTX4, which share a conserved C-terminal region containing the RING and DELTEX C-terminal (DTC) domains (*7, 10*). Whilst the RING domain functions by recruiting E2 thioesterified with Ub (E2~Ub) to catalyse Ub transfer to a substrate (*11*), the DTC domain, which is connected to the RING domain through a short flexible linker remained, until recently, without a reported function. DTX3L, which forms a heterodimer with poly(ADP-ribose) polymerase 9 (PARP9) (*12*), was initially proposed to be an activator of PARP9 ADP-ribosyltransferase activity, with the complex being shown to catalyse ADP-ribosylation of Ub in the presence of nicotinamide adenine dinucleotide (NAD^+) and ubiquitination components including E1, E2, Ub, Mg^{2+} and ATP (*8*). It was originally proposed that PARP9 was responsible for this activity, despite previous reports of its catalytic inactivity (*13*). When we tested DTX3L independently of PARP9, it was sufficient to catalyse ADP-ribosylation of the C-terminus of Ub(*7*). Notably, the C-terminal RING and DTC domains (hereafter referred to as RD domains) are the

59 minimal fragment required to catalyse this reaction and all members of the DTX family share this
60 capability (*7-9*). Structural analyses of RD domains revealed that the DTC domain contains a pocket
61 that binds ADPr and NAD^+ (*7, 10*). This enables RD domains to recruit ADPr-modified substrates and
62 catalyse their ubiquitination in a poly-ADP-ribose (PAR)-dependent manner (*10*). In addition, in the
63 presence of NAD^+ and ubiquitination components, RD domains catalyse ADP-ribosylation of Ub (*7*).
64 The chemical linkage of ADP-ribosylated Ub was recently discovered to occur between the carboxylate
65 group of Ub Gly^{76} and the 3'-hydroxyl group of the adenosine-proximal ribose of ADPr or NAD^+,
66 highlighting Ub modification of ADPr or NAD^+ rather than the canonical ADP-ribosylation of substrate
67 that involves the release of nicotinamide from NAD^+ followed by attachment of ADPr via the C1" atom
68 of the nicotinamide ribose (*9*). Furthermore, recent studies have demonstrated that the RD domains of
69 both DTX2 and DTX3L can ubiquitinate the 3'-hydroxyl group of the adenosine-proximal ribose of
70 free ADPr as well as ADPr moieties present on ADP-ribosylated proteins (*9*) and ADP-ribosylated
71 nucleic acids (*14*).

72

73 DTX3L has a unique N-terminus lacking the WWE domains and proline-rich regions found in the other
74 DTX family members. The development of AlphaFold Protein Structure Database (*15*) has allowed
75 prediction of unsolved protein structures to a higher degree of confidence than previously possible. For
76 DTX3L, this allowed the generation of a model of the protein that revealed putative domains in the N-
77 terminal region. When queried in the DALI server, which enables protein structures to be compared in
78 3D, these domains were found to be structurally similar to K Homology (KH) domains and RNA
79 recognition motifs (RRMs) which bind single-stranded DNA (ssDNA) and RNA (ssRNA). Here, we
80 showed that DTX3L was able to bind a variety of sequences of ssDNA and ssRNA. Unexpectedly, we
81 discovered that DTX3L was able to ubiquitinate ssDNA and ssRNA. Biochemical and structural
82 analyses established that DTX3L-RD domain binds single-stranded nucleic acids (ssNAs) and catalyzes
83 the ubiquitination of ssNAs. These findings present a previously unidentified direct Ub modification of
84 nucleic acids.

85

86 **RESULTS**

87 **DTX3L binds and ubiquitinates ssRNA and ssDNA**

88 To gain insight into the function of DTX3L, we took the AlphaFold-predicted structural domains of
89 DTX3L (Fig. 1A) and conducted a search on the DALI server to compare the proposed 3D domains of
90 DTX3L to structures in the Protein Data Bank (PDB). Several of these domains share structural
91 similarity to KH domains (Fig. 1, B and C) with the N-terminal domain resembling an RRM. KH
92 domains, which bind both ssRNA (*16*) and ssDNA (*17*), comprise a three-stranded anti-parallel β-sheet
93 packed alongside three α-helices whereas RRMs are composed of two α-helices and four anti-parallel
94 strands packed together in a β-α-β-β-α-β fold (*18*). To determine if DTX3L binds ssRNA or ssDNA, we
95 used ssDNA and ssRNA oligonucleotides labelled with 6-FAM on the 5'-end (D1-D9 and R1-R9,
96 respectively; Table 1 and fig. S1A) and either full-length (FL) DTX3L or a truncated 232-C construct
97 containing the two tandem KH-like (KHL) domains and C-terminal RING-DTC that is competent in
98 binding PARP9 (*19*). Both DTX3L constructs bound to all tested sequences of ssRNA and ssDNA,
99 inducing at least a two-fold change in polarisation (Fig. 1, D and E and fig. S1, B and C). Likewise, at
100 least a two-fold change in polarisation was observed when DTX3L-PARP9 complex binding was tested
101 with these nucleic acids, demonstrating that PARP9 does not occlude ssDNA or ssRNA binding by
102 DTX3L (fig. S1, D and E).

103

104 Based on the structural similarity between ADPr and nucleic acids (fig. S1F), we hypothesised that
105 RNA and DNA could also be ubiquitinated by DTX3L. To investigate, we performed *in vitro*
106 ubiquitination assays of FAM-labelled ssDNA or ssRNA by DTX3L with the following components:
107 E1, UBE2D2, Ub, and Mg^{2+}-ATP. Ubiquitination of FAM-labelled ssDNA and ssRNA was detected by
108 SDS-PAGE using a fluorescent scanner (Typhoon FLA7000). The appearance of a ~15 kDa band
109 closely matched the combined molecular weights of Ub (8564 Da) and 20 nt FAM-labelled single-
110 stranded nucleic acid (~6900-7300 Da), suggesting that both ssDNA (Fig. 1F) and ssRNA (Fig. 1G)
111 were ubiquitinated by DTX3L. Due to the high signal-to-noise ratio observed with D4 compared to

112 other oligonucleotides, this sequence was used for subsequent experiments. Because R4 is the
113 corresponding sequence of ssRNA this was also taken forward.
114
115 The minimal fragment of DTX3L required for Ub-ADPr formation is the conserved C-terminal RING-
116 DTC domain (*7*). To investigate the minimal fragment of DTX3L necessary for the ubiquitination of
117 ssNAs, we tracked the formation of ubiquitinated ssDNA (Ub-DNA) or ssRNA (Ub-RNA) by DTX3L
118 232-C, RD, RING or DTC. DTX3L 232-C lacks the N-terminal RRM and KHL1 domains, where KHL1
119 domain was recently proposed to enable oligomerization (*20*). While DTX3L 232-C exhibited reduced
120 autoubiquitination compared to DTX3L FL (fig. S1G), the rates of UBE2D2~Ub discharge were
121 comparable (fig. S1H). This suggests that DTX3L 232-C is catalytically competent as DTX3L FL, but
122 lacks accessible lysine sites necessary for autoubiquitination. DTX3L 232-C exhibited similar activity
123 as DTX3L FL in catalysing the formation of Ub-DNA (Fig. 1H) and Ub-RNA (Fig. 1I). DTX3L-RD
124 also catalysed formation of Ub-DNA (Fig. 1H) and Ub-RNA (Fig. 1I), whereas neither the RING (R)
125 nor the DTC (D) alone sufficed. Hints of the ~15 kDa Ub-DNA band were also observed on the
126 corresponding Coomassie-stained SDS-PAGE gel (fig. S1I, arrows).
127
128 We took advantage of the Coomassie staining method of detection for Ub-DNA, along with an increased
129 concentration of D4, to confirm this and demonstrate that formation of Ub-DNA is time-dependent (Fig.
130 1J). To validate that Ub modification did not occur on the FAM label, we tested ssDNA labelled with
131 IRDye® 800 (D10, Table 1; fig. S1J) and unlabelled ssDNA (D11, Table 1) in a ubiquitination assay. A
132 ~15 kDa band corresponding to the predicted molecular weight of Ub-DNA was also observed using
133 ssDNA with the alternative label (Fig. 1K) and unlabelled ssDNA (Fig. 1L). Together, our data
134 demonstrate that DTX3L binds and ubiquitinates ssNAs and that DTX3L-RD is the minimal fragment
135 required to catalyse this reaction.
136
137 **The 3'-end of ssDNA is modified on its 3' hydroxyl**
138 Based on the finding that the RD was sufficient to catalyse ubiquitination of ssDNA D4, we confirmed
139 that this fragment was able to ubiquitinate the same ssDNAs as FL DTX3L (fig. S1K). Hence, this

140 fragment was used to probe the additional requirements of the reaction. Initially, to confirm that product
141 formation was dependent on the ubiquitination process, we removed each reactant individually.
142 Formation of Ub-DNA or Ub-RNA by DTX3L-RD was only detected when all components of the
143 ubiquitination cascade (E1, UBE2D2, Ub, Mg^{2+}-ATP) were present (Fig. 2, A and B). To validate that
144 ssDNA and ssRNA were modified with Ub and not another component in the reaction, we treated the
145 resulting product with USP2, a promiscuous deubiquitinating enzyme. The ~15 kDa band disappeared
146 upon treatment with USP2, which is consistent with removal of Ub from ssDNA (Fig. 2C) and ssRNA
147 (Fig. 2D) and shows that this modification is reversible. Treatment of Ub-DNA and Ub-RNA with
148 Benzonase, an endonuclease which degrades DNA and RNA, caused the disappearance of both the Ub-
149 DNA and DNA bands (Fig. 2C) and Ub-RNA and RNA bands (Fig. 2D). Poly(ADP-ribose)
150 glycohydrolase (PARG), an ADPr hydrolase that cleaves ADPr-linked to substrate, was recently shown
151 to cleave Ub-ADPr attached to nucleic acid substrates (*14*). Treatment with PARG had no effect on the
152 Ub-DNA band (Fig. 2C) or Ub-RNA band (Fig. 2D), thereby demonstrating that this reaction is distinct
153 from the attachment of Ub to the ADPr moiety on ADP-ribosylated nucleic acids (*14*). These findings
154 showed that the 15 kDa product was ubiquitinated ssNAs.
155
156 Our experiments suggested a common mechanism of modification between ssRNA and ssDNA,
157 therefore we focused our subsequent experiments on the most readily detectable substrate, ssDNA D4.
158 To ascertain whether this reaction was specific to ssDNA, we followed the formation of Ub-DNA with
159 6-FAM-labelled dsDNA and DTX3L-RD. Based on the finding that the RD fragment was sufficient to
160 catalyse ubiquitination of ssDNA, this fragment was used to probe the additional requirements of the
161 reaction. DTX3L-RD did not ubiquitinate dsDNA (D12, Table 1; Fig. 2E) suggesting that the protein is
162 specific for ssDNA. We then compared ubiquitination of ssDNA labelled with 6-FAM on the 5'-end or
163 3'-end (D13, Table 1; fig. S1, A and L) and found that the 6-FAM label on the 3'-end blocked
164 ubiquitination of ssDNA (Fig. 2F). Based on this finding we hypothesised that the 3' end of the
165 oligonucleotide is (1) the site of modification or (2) important for oligonucleotide binding. We next
166 investigated the chemical nature of the covalent bond between Ub and ssDNA. To see if the bond was
167 hydrolysed under basic conditions, we treated our reaction with pH 9.5 buffer which led to the

168 disappearance of the Ub-DNA band over time (Fig. 2G). Additionally, treatment with NH_2OH resulted
169 in the rapid disappearance of the Ub-DNA band (Fig. 2H). Together, this suggested that the linkage is
170 likely to be an ester, and that the modification occurs on a ribose moiety, leaving only the 3' ribose as a
171 viable modification site. To validate this hypothesis, we designed an array of 5'-FAM labelled ssDNAs
172 in which various positions on the ribose ring of the 3'-end nucleotide were modified and tested their
173 ability to act as a substrate for ubiquitination by DTX3L-RD. Whilst ssDNA with a fluorine atom
174 attached at the 2' position of the ribose ring (D14) was ubiquitinated, the addition of a phosphate moiety
175 to the 3' hydroxyl of the ribose ring (D15) ablated the formation of Ub-DNA, thereby confirming this
176 is the site of modification (D10, D14-D15, Table 1; Fig. 2I). This is consistent with the site of Ub
177 modification of ADPr where Ub is also attached to the 3' hydroxyl of the adenine-proximal ribose (*9*).
178 These data support that Ub modification of ssDNA occurs at the 3' hydroxyl of the 3' nucleotide.
179
180 **Nucleotide sequence requirements for Ub-DNA formation**
181 How the sequence and length of ssDNA affect Ub-DNA formation is unclear. To investigate, we first
182 probed the base preference at the last or penultimate position by varying the nucleic acid to A, T, C or
183 G of oligonucleotide D4. Whilst only the sequences ending with A and to some extent with G could be
184 ubiquitinated by DTX3L-RD, the requirement for the penultimate nucleotide was less strict, with
185 sequences ending CA, TA and AA all being ubiquitinated (D16-D21, Table 1; Fig. 3, A and B). Thus far
186 we had only tested sequences of 20 nucleotides in length; therefore, we next took the D4 sequence and
187 generated four ssDNA nucleotides with this same CAA repeat unit and ranging in length from five to
188 80 nucleotides (D22-D25, Table 1). When tested in our assays, all four of these nucleotide substrates
189 were ubiquitinated (Fig. 3, C and D). Despite dsDNA being unable to act as a substrate for
190 ubiquitination, our discovery that ubiquitination occurs on the 3' nucleotide of ssDNA prompted us to
191 test the hypothesis that dsDNA with a 3' overhang could be ubiquitinated. Whilst dsDNA with a single
192 3' nucleotide overhang could not be ubiquitinated, dsDNA with a two or three 3' nucleotide overhang
193 could be modified with Ub (D26-D29, Table 1; Fig. 3E). Our data show that DTX3L modification of
194 DNA requires that the two nucleotides at the 3' end be single-stranded. Overall, these data demonstrate
195 the ability of DTX3L-RD to ubiquitinate ssDNA of varying lengths and specific 3' dinucleotides.

196

197 **ssNA and ADPr share a binding site on DTX3L's DTC domain**

198 Because the modification of ssDNA and ADPr occurs at the same position on the nucleoside, we next
199 explored the possibility that they share the same binding site on DTX3L-RD. ADPr binds the DTC
200 domain of DTX2 (*10*), a region which is conserved in the DTX family. Therefore, we purified ^{15}N-
201 DTX3L-RD and acquired ^{1}H-^{15}N heteronuclear single-quantum coherence (HSQC) spectra of ^{15}N-
202 DTX3L-RD alone and in the presence of ADPr or unlabelled ssDNA. We utilised the unlabelled version
203 of the 5-mer oligonucleotide ssDNA (D30, Table 1) for NMR analysis, which was sufficient to produce
204 the Ub-DNA product (Fig. 3C). Upon titration of ADPr or 5-nucleotide ssDNA, chemical shift
205 perturbations (CSPs) occurred, indicating DTX3L-RD binds both ADPr and ssDNA (Fig. 4A and fig.
206 S2, A and B). The similarity in the CSPs indicates that there is some overlap in the binding sites of
207 ADPr and ssDNA (Fig. 4, A–C). To further verify that there is conservation between the binding sites
208 of these two substrates, excess ADPr was added to the ubiquitination reaction components along with
209 DTX3L-RD and ssDNA D4. The presence of ADPr inhibited the formation of Ub-DNA and Ub-RNA
210 (Fig. 4D and fig. S2C), suggesting they share the same binding site. We next added excess ssDNA D31,
211 a ssDNA with the same sequence as D4 but with a phosphate moiety attached to the 3' hydroxyl, to the
212 ubiquitination reaction components along with DTX3L-RD and biotin-NAD^{+}. As labelled ADPr is not
213 readily available, we used biotin-NAD^{+} to monitor Ub-biotin-NAD^{+} formation. The addition of D31
214 inhibited the formation of Ub-NAD^{+} (Fig. 4E). Because D31 has a phosphate moiety blocking the 3'
215 hydroxyl ubiquitination site, it cannot be ubiquitinated; therefore, it must be directly competing for
216 binding.

217

218 To assess DTX3L-RD preference for nucleic acid or ADPr, we performed kinetic analysis of Ub-D4
219 and Ub-F-NAD^{+} formation by DTX3L-RD using D4 and 6-Fluo-10-NAD^{+} (F-NAD^{+}), respectively, as
220 substrates. DTX3L-RD displayed a k_{cat} value of 0.0358 ± 0.0034 min^{-1} and a K_m value of 6.56 ± 1.80
221 μM for Ub-D4 formation, whereas the Michaelis-Menten curve did not reach saturation for Ub-F-NAD^{+}
222 formation (Fig. 4F and fig. S2, D-G). Comparison of the estimated catalytic efficiency (k_{cat}/K_m = 5457

223 M^{-1} min^{-1} for D4 and estimated k_{cat}/K_m = 1190 M^{-1} min^{-1} for F-NAD^+; Fig. 4F) suggested that DTX3L-
224 RD exhibited 4.5-fold higher catalytic efficiency for D4 than F-NAD^+. This difference primarily results
225 from a better K_m value for D4 compared to F-NAD^+. Although DTX3L-RD showed weak K_m for F-
226 NAD^+, it displays a higher rate for converting F-NAD^+ to Ub-F-NAD^+ at higher substrate concentration
227 (Fig. 4F). Thus, substrate concentration will play a role in determining the preference.
228
229 Previously, we demonstrated the importance of DTX2 His^{594} located in the DTC pocket for the
230 interaction with ADPr (Fig. 4G) (*10*). We examined the effect of mutating the corresponding residue
231 (Tyr^{719}) in DTX3L (Fig. 4H) and found that the Y719A mutant was defective in ubiquitination of ssDNA
232 (Fig. 4I). Two catalytic residues in the DTC domain of DTX2(*9*), His^{582} and Glu^{608}, have been
233 previously identified as important for the ubiquitination of ADPr, and are conserved across the DTX
234 family members (Fig. 4, G and H and fig. S3A). Based on the similarities in mechanism and
235 conservation of the binding site between ADPr and ssDNA, we next investigated if these catalytic
236 residues were involved in the ubiquitination of ssDNA. Substitution of His^{707} by alanine in FL DTX3L
237 completely abolished the formation of Ub-DNA, whilst substitution of Glu^{733} by alanine considerably
238 impaired product formation (Fig. 4I). To test whether this mechanism was conserved across ssNAs, we
239 repeated the mutant DTX3L ubiquitination assay with ssRNA R4 and found similar results (fig. S2H).
240 Overall, the data support the idea that DTX3L utilises the ADPr-binding pocket and the same catalytic
241 residues in the DTC domain to bind and catalyse ubiquitination of ssNAs.
242
243 **Ubiquitination of ssDNA is unique to DTX3 and DTX3L**
244 Since the DTC domains are conserved between DTX family members and share the ability to
245 ubiquitinate ADPr (*7*), we tested whether ubiquitination of ssDNA was a universal feature of the DTX
246 family. Unexpectedly, only DTX3L and to a lesser extent DTX3 were able to ubiquitinate ssDNA under
247 our assay conditions (Fig. 5, A–D). Several potential explanations were considered for this preference:
248 (1) other DTX DTCs might not bind ssDNA; (2) other DTXs might favour different sequences of
249 ssDNA; (3) or the arrangement of the RING and DTC domains in relation to each other might play a
250 crucial role in catalysis. To probe this further, we titrated DTX3L-RING with excess DTX3L-DTC and

251 tracked the formation of Ub-DNA, comparing the ability of the separate domains to ubiquitinate DNA
252 *in trans* with that of DTX3L-RD. No ubiquitination of ssDNA was observed even at a 10:1 molar ratio
253 of DTC to RING domain (Fig. 5E), indicating that the ubiquitination of ssDNA only occurs at an
254 appreciable rate *in cis*. Next, we examined whether DTX2 could catalyse the ubiquitination of ssDNA
255 using 9 different ssDNA sequences and found that DTX2 was unable to ubiquitinate them (Fig. 5F).
256 Lastly, we produced domain-swapped variants of DTX2 and DTX3L in which their respective RING
257 and DTC domains were swapped ($DTX2^R$-$DTX3L^D$ and $DTX3L^R$-$DTX2^D$) and examined the ability of
258 these chimeras to ubiquitinate biotin-NAD^+ or ssDNA D4. We hypothesised that the DTX3L DTC
259 domain of $DTX2^R$-$DTX3L^D$ would be sufficient to enable binding and ubiquitination of ssDNA. Both
260 chimeras were competent in performing ubiquitination of biotin-NAD^+ (Fig. 5G) but were unable to
261 produce Ub-DNA (Fig. 5H). These results suggest that the specific arrangement of the RING and DTC
262 domains in DTX3L is crucial in specifying Ub modification of ssDNA. Taken together, we propose a
263 mechanism for the ubiquitination of ssNAs by the DTX3L-RD domains (Fig. 5I): the DTC domain
264 binds ssNAs, the RING domain recruits E2~Ub, and the RD domains bring the thioester linked Ub into
265 proximity with the 3' end of ssNA. This allows the catalytic residues in the DTC domain to enable the
266 covalent attachment of Ub to the 3' hydroxyl group on the 3'-end of ssNA. Subsequently, the complex
267 dissociates, releasing ssNA-Ub. The substrates for the DTC domain also include ADPr, NAD^+, and
268 ADPr-modified nucleic acids and proteins.
269

270 **DISCUSSION**

271 The diversity of non-proteinaceous substrates that have been demonstrated to undergo ubiquitination
272 has been steadily expanding over the last few years (*5, 7, 21*). Here, we report additional examples of
273 non-canonical substrates, namely ssRNA, ssDNA and dsDNA with a 3' overhang of at least two
274 nucleotides, that undergo ubiquitination by DTX3L. Our biochemical and NMR analyses show that the
275 DTX3L DTC domain binds ssNAs, whilst the RING domain is required for formation of the Ub-NA
276 product. Mutational studies herein reveal three residues, His^{707}, Tyr^{719} and Glu^{733}, within the DTC
277 domain that are required for the formation of Ub-NA. These residues are conserved within the DTC
278 domain, are known to coordinate ADPr (*7, 10*) and are proposed to constitute a catalytic triad essential

279 for DTX E3-mediated ubiquitination of ADPr (*9*). These findings, coupled with knowledge that the 3'-
280 hydroxyl of the nucleotide ribose is the modification site, suggest a potential similarity in the
281 mechanism of Ub modification of ssDNA, ssRNA, and ADPr by DTX3L.

282

283 The chemical structures of ssNAs and ADPr share a ribose-5-phosphate moiety and potentially an
284 adenine base, depending on the ssNA sequence. While our data suggest that DTX3L prefers to
285 ubiquitinate ssDNA ending with adenosine and to some extent guanosine – both purine bases,
286 pyrimidine bases are also tolerated. This raises uncertainty about how DTX3L DTC binds ssNA. Our
287 experiments with dsDNA with a 3' overhang in one strand showed that dsDNA with a single nucleotide
288 overhang cannot be ubiquitinated, whereas dsDNA with a two-nucleotide overhang was ubiquitinated.
289 Notably, alterations in the sequence of the last two nucleotides at the 3' end influenced Ub-DNA product
290 formation (Fig. 3, A and B). These observations suggest that the DTX3L DTC NA-binding pocket may
291 accommodate a dinucleotide. Upon examining the ssDNA sequences utilised in our study (Fig. 1F and
292 3A; Table 1), it appears that the DTX3L DTC pocket might accommodate diverse sequences in the last
293 two nucleotides at the 3' end, with adenine being the preferred last nucleotide and cytosine being the
294 least favoured. Despite the sequence conservation of the RING-DTC domain with other DTX proteins,
295 our biochemical data revealed that only DTX3L and DTX3 were able to ubiquitinate ssDNA. A
296 comparison of the aligned sequences of the DTX RING-DTC domains reveals some differences (fig.
297 S3A). The RING domains of DTX3L and DTX3 lack insertions found in DTX1, DTX2 and DTX4,
298 making their RING domains appear smaller (fig. S3, A–C). Furthermore, DTX3L and DTX3 lack an
299 AR motif found near the DTC pocket. The absence of the AR motif causes a slight conformational
300 change near the DTC pocket, resulting in an extended β-strand and the loss of a bulge containing the
301 arginine residue (fig. S3, A, D, E). Consequently, DTX3L has an extended groove adjacent to the DTC
302 pocket that could accommodate one or more of the nucleotides 5' to the targeted terminal nucleotide.
303 Replacing DTX2-RD's DTC domain with that of DTX3L produced a chimeric construct that was able
304 to ubiquitinate NAD^+ but not ssDNA (Fig. 5, G and H), suggesting that additional factors beyond the
305 catalytic residues and ssDNA binding properties of the DTC domain likely play a role in ubiquitination.

306 Our findings show that this reaction only occurs *in cis*, pointing to the orientation of the RING relative
307 to the DTC domain as an important feature in the formation of Ub-DNA. Future structural
308 characterisation of DTX3L-RD binding to ssDNA or ssRNA should provide insights into its binding
309 mode and sequence selectivity, thereby potentially revealing whether the biological substrate is ssDNA,
310 ssRNA or both.

311

312 Typically, KH domains contain a GXXG motif within the loop between the first and second α helix
313 (*22*). However, analysis of the sequence of the KHL domains in DTX3L shows these domains lack this
314 motif. Multiple studies have shown that mutation in this motif abolishes binding to nucleic acids (*23-*
315 *26*). Our findings show the DTX3L DTC domain binds nucleic acids but whether the KHL domains
316 contribute to nucleic acid binding requires further investigation. Additionally, the structure of the first
317 KHL domain was recently reported and shown to form a tetrameric assembly (*20*). Our analysis with
318 DTX3L 232-C, which lacks the first KHL domain and RRM, indicate that it can still bind ssDNA and
319 ssRNA. Despite this, a more detailed analysis will be required to determine whether oligomerization
320 plays a role in nucleic acid binding and ubiquitination.

321

322 In recent years, several studies have unveiled diverse reactions catalysed by DTX3L. It forms a
323 heterodimeric complex with PARP9, facilitating the direct ubiquitination of substrates such as H2B
324 (*27*). This complex can recruit PARylated substrates, either through PARP9 macrodomains (*27*) or
325 DTX3L DTC domain (*10*), for direct substrate ubiquitination. Notably, it can catalyse the transfer of
326 Ub to NAD^+ or ADPr (*7-9*), including ADPr moieties of PARylated substrates, encompassing both
327 proteins and nucleic acids (*9*). Moreover, we have expanded its substrate repertoire by demonstrating
328 its ability to directly ubiquitinate the 3' end of ssNAs. Whether this reaction occurs in cells and what
329 the native substrate (RNA, DNA or both) are yet to be determined. Due to the labile nature of the ribose
330 ester bond and cleavage of Ub conjugates by DUBs, as well as the digestion of nucleic acids by
331 nucleases, our ability to probe the Ub modification of ssNAs in a cellular context has so far been limited.
332 Connecting these chemical reactions to precise biological functions requires carefully designed

333 experiments aimed at distinguishing these functions. Based on the known functions of the
334 DTX3L/PARP9 complex and the findings of this study, we propose several hypotheses for future
335 research. The DTX3L/PARP9 complex has a known involvement in DNA damage repair, utilising
336 PARP9's macrodomains to recognise PAR and assist in complex recruitment to the damaged foci (*8*).
337 RNA itself contributes to DNA damage repair (*28*). Likewise, these damage sites may involve DNA
338 breaks with 3' overhangs. Our findings reveal that DTX3L can recognise and ubiquitinate ssRNA, or
339 dsDNA with a 3' overhang of two or more nucleotides. This observation suggests a possible substrate
340 for DTX3L in DNA damage repair pathways, which requires further investigation. In eukaryotic cells,
341 messenger RNA (mRNA) is a source of ssRNA that commonly possesses a poly-A tail at the 3' end.
342 Our data indicated that DTX3L can ubiquitinate ssRNA containing a poly-A sequence (Fig. 1G, lane
343 R9), offering a possibility for future exploration. Viruses contain a diverse range of genetic materials
344 including ssNAs, which might be plausible ubiquitination targets. Studies have shown that expression
345 of DTX3L/PARP9 complex is induced after viral infection, and the complex plays a role in antiviral
346 defense mechanisms by ubiquitinating both host and viral proteins (*27, 29*). Ubiquitination of viral
347 ssNAs by DTX3L presents another intriguing hypothesis for future research.

348 Our study reports the first example of direct ubiquitination of ssNAs by DTX3L and illustrates the
349 possibility of additional roles for ubiquitination beyond that of a conventional post-translational
350 modification.

351

352 **Materials And Methods**

353 **Construct generation**

354 Constructs were generated by standard polymerase chain reaction–ligation techniques and verified by
355 automated sequencing. GST-tagged constructs were cloned into a modified form of pGEX4T-3 (GE
356 Healthcare) with a TEV cleavage site and a second ribosomal binding and multiple cloning site (pABLO
357 TEV) and His-tagged constructs were cloned into a modified form of pRSF_Duet-1 (Novagen) with a
358 TEV cleavage site following the hexahistidine tag. All proteins are from human sequences. RD domains

359 are comprised of residues 388-C of DTX1, residues 390-C of DTX2, residues 148-C of DTX3, residues
360 387-C of DTX4 and residues 544-C of DTX3L. DTC of DTX3L comprises residues 607-C. PARG
361 comprises residues 448-C. USP2 comprises residues 260-C. The complex, DTX3L(232-
362 C)/PARP9(509-C), was cloned into a bicistronic vector in which PARP9(509-C) was cloned into the
363 first MCS of pRSF_Duet-1 with an N-terminal His-MBP tag followed by a TEV cleavage site, and
364 DTX3L(232-C) was cloned into the second MCS untagged. DTX3L 232-C and PARP9 509-C were
365 sufficient to form complex (*27*). DTX3L FL and DTX3L 232-C were cloned into pABLO vector.
366
367 **Protein expression and purification**
368 Expression of recombinant proteins was conducted in *Escherichia coli* BL21(DE3) Gold or
369 Rosetta2(DE3) pLysS cells. Cultures were grown in LB broth (Miller) at 37 °C until an OD_{600} of 0.6-
370 0.8 was reached at which point expression was induced with 0.2 mM isopropyl β-D-1-
371 thiogalactopyranoside (IPTG) at 20 °C for 12-16 hours. ^{15}N-labelled DTX3L-RD was obtained using
372 M9 minimal medium. Briefly, 20 mL starter cultures were grown in LB medium overnight before cells
373 were pelleted and washed in M9 medium. Each pellet was added to 1L of M9 medium supplemented
374 with: 1 g of $^{15}NH_4Cl$, 5 g glucose, 50 mg kanamycin, 1X Vitamin Stock (Gibco), 1 mg D-Biotin and
375 trace metals. Cells were grown until an OD_{600} of 0.6-0.8 was reached at which point expression was
376 induced with IPTG at 20 °C for 20 hours.
377 Cells were harvested by centrifugation following expression and lysed by microfluidizer or sonicator.
378 Cells expressing GST-tagged proteins were resuspended in 50 mM Tris-HCl (pH 7.6), 200 mM NaCl
379 and 1 mM DTT. Cells expressing His-tagged proteins were resuspended in 25 mM Tris-HCl (pH 7.6),
380 200 mM NaCl, 15 mM imidazole, 5 mM beta-mercaptoethanol. Cell lysates were cleared by high-speed
381 ultracentrifugation. Clarified lysates were applied to glutathione affinity or Ni^{2+}-agarose by incubating
382 for 1 to 2 hours on a rotary shaker at 4°C or using a gravity column. Beads were washed in buffers
383 similar to lysis buffer. ^{15}N-DTX3L-RD was eluted with 6xHis intact in 25 mM Tris-HCl (pH 7.6), 200
384 mM NaCl, 5 mM BME, and 200 mM imidazole, then further purified by ion exchange chromatography,
385 followed by size exclusion chromatography on a Superdex 75 column (GE Healthcare) into buffer

386 containing 20 mM sodium phosphate, (pH 7.0), 100 mM NaCl, 0.02% NaN_3 and 1 mM TCEP before
387 snap-freezing in liquid nitrogen and storing at −80 °C.
388 For removal of the GST tag, protein samples were dialysed against 25 mM Tris-HCl (pH 7.6), 150 mM
389 NaCl, and 5 mM BME overnight at 4 °C in the presence of TEV protease or alternatively cleaved on
390 the beads with TEV from a glutathione agarose column in 50 mM Tris-HCl (pH 8.0), 200 mM NaCl,
391 and 5 mM DTT. The dialysed and cleaved samples were loaded onto the same resin and flow through
392 collected to separate from the affinity tags or the remaining uncleaved proteins. Additional purification
393 was performed by size exclusion chromatography on a Superdex 75 column or Superdex 200 column
394 (GE Healthcare), depending on protein size, into 25 mM Tris-HCl (pH 7.6), 150 mM NaCl, and 1 mM
395 DTT before snap-freezing in liquid nitrogen and storing at −80 °C. Protein concentrations were
396 determined using Bio-RAD protein assay.
397 DTX3L (232-C)/PARP9 (509-C) complex was obtained by expressing the bicistronic construct of His-
398 MBP-PARP9(509-C)/DTX3L(232-C). The complex was purified by Ni^{2+}-agarose, cleaved by TEV
399 treatment, loaded back on Ni^{2+} for tag and protease removal, and further purified by Source S cation
400 exchange chromatography and Superdex 200.
401 Additional proteins: *Arabidopsis thaliana* Uba1 (*30, 31*), UBE2D2 (*30, 32*), Ub (*30, 33*), PARG (*7*)
402 and USP2 (*34*) were purified as in previously described protocols.
403
404 **Oligonucleotides**
405 Oligonucleotides were obtained from Integrated DNA Technologies and are listed in Table 1.
406
407 **Fluorescence polarisation assay**
408 50 nM 6-FAM-labelled nucleic acids (Integrated DNA Technologies) were incubated with 0-5 μM
409 proteins in reaction buffer (20 mM Hepes pH 7.0, 1 mM $MgCl_2$, 50 mM NaCl, filter sterilised).
410 Fluorescence polarisation measurements were taken using Tecan Spark (λex=485 nm, λem=535 nm).
411 Fold change was calculated based on the change in polarisation compared to the fluorescent ligand in
412 the absence of protein. Data were plotted in Prism (GraphPad).
413

414 **DNA and RNA ubiquitination assays**

415 UBA1 (0.2 μM), UBE2D2 (5 μM) and Ub (50 μM) were incubated in 50 mM Tris-HCl, 5 mM $MgCl_2$,
416 50 mM NaCl and 5 mM ATP at room temperature for 15 minutes to allow for generation of E2~Ub.
417 DTX (1 μM) and nucleic acid (3 μM) were incubated together at room temperature for 10 minutes prior
418 to mixing with other components. After components were combined, reactions were incubated at 37 °C.
419 Aliquots were taken immediately (indicated by 0.2 min time point) and at specified subsequent time
420 points. The reactions were halted by addition of 2X Loading Dye containing 250 mM DTT and resolved
421 by SDS-PAGE (NuPAGE 4-12% Bis-Tris, Invitrogen). For FAM-labelled nucleic acids, gels were
422 visualised using Typhoon FLA 700 with λex=473 nm and Y520 emission filter (Cytiva Life Sciences).
423 For IRDye 800 labelled nucleic acids, gels were scanned with an Odyssey CLx Imaging System (LI-
424 COR Biosciences). For Fig. 1J and 5, A, B, C and D, 25 μM D4 was used. For Fig. 1L, 25 μM D11 was
425 used. For assays with USP2, Benzonase and PARG, reactions were conducted as above and after UBA1
426 (0.2 μM), UBE2D2 (5 μM), Ub (50 μM), DTX3L-RD (2 μM) and D4 or R4 (2 μM) were incubated
427 together for 30 minutes, reactions were quenched with 250 mM DTT and buffer exchanged into 25 mM
428 Tris-HCl (pH 7.6), 150 mM NaCl, 5 mM $MgCl_2$ and 1 mM DTT using a 7 kDa Zeba Spin column.
429 USP2 (1.35 μM), Benzonase (1 μM) or PARG (1 μM) was added and incubated for a further 30 minutes
430 at 37 °C. Subsequently, an aliquot was mixed with 2X Loading Dye and resolved by SDS-PAGE. For
431 assays conducted at pH 9.5, reactions were conducted as above and after UBA1 (0.2 μM), UBE2D2 (5
432 μM), Ub (50 μM), DTX3L-RD (1 μM) and D4 (3 μM) were incubated together for 30 minutes, reactions
433 were quenched with 250 mM DTT and buffer exchanged into 25 mM Tris-HCl (pH 9.5), 150 mM NaCl
434 and 1 mM DTT using a 7 kDa Zeba Spin column. Then 2 mM EDTA was added, and the reaction was
435 incubated at 37 °C. Aliquots were taken at indicated time points, mixed with 2X Loading Dye, and
436 resolved by SDS-PAGE. For assays conducted with NH_2OH treatment, reactions were conducted as
437 above and after UBA1 (0.2 μM), UBE2D2 (5 μM), Ub (50 μM), DTX3L-RD (1 μM) and D4 (3 μM)
438 were incubated together for 30 minutes. Reactions were quenched with 250 mM DTT and buffer
439 exchanged into 25 mM Tris-HCl (pH 9), 150 mM NaCl and 1 mM DTT using a 7 kDa Zeba Spin
440 column. Then 1.5 M NH_2OH was added, and the reaction was incubated at 37 °C. Aliquots were taken
441 at indicated time points, mixed with 2X Loading Dye, and resolved by SDS-PAGE.

442

443 **Autoubiquitination assay**

444 UBA1 (0.2 μM), UBE2D2 (5 μM) and fluorescently-labelled Ub (*35*) (25 μM) were incubated in 50
445 mM Tris-HCl, 5 mM $MgCl_2$, 50 mM NaCl and 5 mM ATP at room temperature for 15 minutes to allow
446 for generation of E2~Ub. DTX3L (1 μM) was added and reactions were incubated at 20 °C. Aliquots
447 were taken at indicated time points, reactions halted by addition of 2X Loading Dye and resolved by
448 SDS-PAGE. Gels were scanned with an Odyssey CLx Imaging System.

449

450 **Lysine discharge assay**

451 UBA1 (0.5 μM), UBE2D2 (25 μM) and Ub (25 μM) were incubated in 50 mM Tris-HCl, 5 mM $MgCl_2$,
452 50 mM NaCl and 5 mM ATP at room temperature for 15 minutes to allow for generation of E2~Ub.
453 Charged reactions were stopped with 30 mM EDTA and T0 sample taken. DTX3L (1 μM) and lysine
454 (300 mM) were added, and reactions were incubated at room temperature. Aliquots were taken at
455 indicated time points, reactions halted by addition of 2X Loading Dye and resolved by SDS-PAGE.
456 Gels were scanned with a ChemiDoc (BioRad).

457

458 **Competition ubiquitination assays**

459 UBA1 (0.2 μM), UBE2D2 (5 μM) and Ub (50 μM) were incubated in 50 mM Tris-HCl, 5 mM $MgCl_2$,
460 50 mM NaCl and 5 mM ATP at room temperature for 15 minutes to allow for generation of E2~Ub.
461 DTX3L-RD (1 μM) and D4 (3 μM) were incubated together at room temperature for 10 minutes prior
462 to mixing with other components. After components were combined, 1 mM ADPr was added and
463 reactions were incubated at 37 °C. Aliquots were taken at indicated time points, reactions were halted
464 by addition of 2X Loading Dye containing 250 mM DTT and resolved by SDS-PAGE. Gels were
465 visualised using Typhoon FLA 700 with λex=473 nm and Y520 emission filter. For Fig. 4E, DTX3L-
466 RD (1 μM) and biotin-NAD^+ (5 μM) were incubated together at room temperature for 10 minutes prior
467 to mixing with other components. After components were combined, 2 mM D31 was added and
468 reactions were incubated at 30 °C. Aliquots were taken at indicated time points, reactions were halted
469 by addition of 2X Loading Dye containing 250 mM DTT and resolved by SDS-PAGE. The samples

470 were transferred to nitrocellulose membrane and blocked in 5% BSA. Membranes were incubated with
471 DyLight 800 conjugated NeutrAvidin (Thermo Fisher Scientific, cat. no. 22853; 1:10,000) and
472 visualised using an Odyssey CLx Imaging System.
473
474 **Kinetic analysis of Ub-D4 and Ub-F-NAD+ formation**
475 UBA1 (0.2 μM), UBE2D2 (5 μM) and Ub (50 μM) were incubated in 50 mM Tris-HCl, 5 mM $MgCl_2$,
476 50 mM NaCl and 5 mM ATP at room temperature for 15 minutes to allow for generation of E2~Ub.
477 DTX (1 μM) and D4 or F-NAD^+ (Biolog Life Science Institute, cat. no. N 023) at varying concentrations
478 (0-37.5 μM) were incubated together at room temperature for 10 minutes prior to mixing with other
479 components. Aliquots were taken after 15 minutes, reactions were halted by addition of 2X Loading
480 Dye containing 250 mM DTT and resolved by SDS-PAGE. Gels were visualised using Typhoon FLA
481 700 with λex=473 nm and Y520 emission filter. A known amount of D4 was visualised on the gel
482 alongside D4 ubiquitination reactions. A known amount of F-NAD^+ was pipetted onto Whatman filter
483 paper and scanned alongside gel of F-NAD^+ ubiquitination reactions. Ub-D4 and Ub-F-NAD^+ were
484 quantified and initial rates expressed as nmoles of product formed per minute per moles of DTX3L-
485 RD. Data from two independent experiments were fitted to the Michaelis-Menten equation using Prism.
486 The Michaelis-Menten curve for Ub-F-NAD^+ was not saturated therefore k_{cat}/K_m was estimated from
487 the slope of the linear portion of the curve.
488
489 **Biotin-NAD^+ ubiquitination assay**
490 UBA1 (0.2 μM), UBE2D2 (5 μM), and Ub (50 μM) were incubated in 50 mM HEPES-NaOH, pH 7.5,
491 5 mM $MgCl_2$, 50 mM NaCl and 5 mM ATP at room temperature for 10 minutes to allow for generation
492 of E2~Ub. DTX (1 μM), NAD^+ (200 μM) and biotin-NAD^+ (10 μM) were added and reactions were
493 incubated at 20 °C for one hour. Reactions were halted by addition of 3X Loading Dye containing 250
494 mM DTT and resolved by SDS-PAGE. The samples were transferred to nitrocellulose membrane and
495 blocked in 5% BSA. Membranes were incubated with DyLight 800 conjugated NeutrAvidin (Thermo
496 Fisher Scientific, cat. no. 22853; 1:10,000) and visualised using an Odyssey CLx Imaging System.
497

498 **Solution NMR experiments**

499 All NMR data were acquired using a Bruker Avance III 600-MHz spectrometer equipped with a
500 cryogenic triple resonance inverse probe. DTX3L-RD samples were prepared at ~100 μM in 20 mM
501 sodium phosphate, (pH 7.0), 100 mM NaCl, 0.02% NaN_3, 1 mM TCEP and 5% D_2O with 0.00025%
502 TSP. Experiments were carried out at 298 K, and ^{1}H-^{15}N HSQC spectra were recorded with 16 scans
503 using 200 complex points with a sweep width of 36 parts per million (ppm) in the ^{15}N dimension. All
504 spectra were processed with 256 points in the indirect dimension using Bruker TopSpin 3.5 and analysed
505 using CcpNmr AnalysisAssign (*36*).

506
507
508 **References**
509

510 1. R. Yau, M. Rape, The increasing complexity of the ubiquitin code. *Nat. Cell Biol.* **18**, 579-586
511 (2016).
512 2. X. Wang, R. A. Herr, M. Rabelink, R. C. Hoeben, E. J. H. J. Wiertz, T. H. Hansen, Ube2j2
513 ubiquitinates hydroxylated amino acids on ER-associated degradation substrates. *J. Cell Biol.*
514 **187**, 655-668 (2009).
515 3. Y. Shimizu, Y. Okuda-Shimizu, L. M. Hendershot, Ubiquitylation of an ERAD Substrate
516 Occurs on Multiple Types of Amino Acids. *Mol. Cell* **40**, 917-926 (2010).
517 4. X. Wang, R. A. Herr, W. J. Chua, L. Lybarger, E. J. Wiertz, T. H. Hansen, Ubiquitination of
518 serine, threonine, or lysine residues on the cytoplasmic tail can induce ERAD of MHC-I by
519 viral E3 ligase mK3. *J. Cell Biol.* **177**, 613-624 (2007).
520 5. E. G. Otten *et al.*, Ubiquitylation of lipopolysaccharide by RNF213 during bacterial infection.
521 *Nature* **594**, 111-116 (2021).
522 6. I. R. Kelsall *et al.*, HOIL-1 ubiquitin ligase activity targets unbranched glucosaccharides and is
523 required to prevent polyglucosan accumulation. *EMBO J.* **41**, e109700 (2022).
524 7. C. Chatrin *et al.*, Structural insights into ADP-ribosylation of ubiquitin by Deltex family E3
525 ubiquitin ligases. *Sci. Adv.* **6**, eabc0418 (2020).
526 8. C. S. Yang *et al.*, Ubiquitin Modification by the E3 Ligase/ADP-ribosyltransferase
527 Dtx3L/Parp9. *Mol. Cell* **66**, 503-503 (2017).
528 9. K. Zhu *et al.*, DELTEX E3 ligases ubiquitylate ADP-ribosyl modification on protein substrates.
529 *Sci. Adv.* **8**, eadd4253 (2022).
530 10. S. F. Ahmed *et al.*, DELTEX2 C-terminal domain recognizes and recruits ADP-ribosylated
531 proteins for ubiquitination. *Sci. Adv.* **6**, eabc0629 (2020).
532 11. R. J. Deshaies, C. A. Joazeiro, RING domain E3 ubiquitin ligases. *Annu. Rev. Biochem.* **78**,
533 399-434 (2009).
534 12. K. Takeyama *et al.*, The BAL-binding Protein BBAP and Related Deltex Family Members
535 Exhibit Ubiquitin-Protein Isopeptide Ligase Activity. *J. Biol. Chem.* **278**, 21930-21937 (2003).
536 13. S. Vyas *et al.*, Family-wide analysis of poly(ADP-ribose) polymerase activity. *Nat. Commun.*
537 **5**, (2014).
538 14. K. Zhu *et al.*, DELTEX E3 ligases ubiquitylate ADP-ribosyl modification on nucleic acids.
539 *Nucleic Acids Res.* **52**, 801-815 (2024).
540 15. J. Jumper *et al.*, Highly accurate protein structure prediction with AlphaFold. *Nature* **596**, 583-
541 589 (2021).

16. J. L. Baber, D. Libutti, D. Levens, N. Tjandra, High Precision Solution Structure of the C-terminal KH Domain of Heterogeneous Nuclear Ribonucleoprotein K, a c-myc Transcription Factor. *J. Mol. Biol.* **289**, 949-962 (1999).
17. J. L. Baber, D. Levens, D. Libutti, N. Tjandra, Chemical Shift Mapped DNA-Binding Sites and 15N Relaxation Analysis of the C-Terminal KH Domain of Heterogeneous Nuclear Ribonucleoprotein K. *Biochemistry* **39**, 6022-6032 (2000).
18. A. Cléry, M. Blatter, F. H. T. Allain, RNA recognition motifs: boring? Not quite. *Curr. Opin. Struct. Biol.* **18**, 290-298 (2008).
19. Y. Ashok *et al.*, Reconstitution of the DTX3L–PARP9 complex reveals determinants for high-affinity heterodimerization and multimeric assembly. *Biochem. J.* **479**, 289-304 (2022).
20. C. Vela-Rodríguez *et al.*, Oligomerization mediated by the D2 domain of DTX3L is critical for DTX3L-PARP9 reading function of mono-ADP-ribosylated androgen receptor. *Protein Sci.* **33**, e4945 (2024).
21. I. R. Kelsall, J. Zhang, A. Knebel, J. S. C. Arthur, P. Cohen, The E3 ligase HOIL-1 catalyses ester bond formation between ubiquitin and components of the Myddosome in mammalian cells. *Proc. Natl. Acad. Sci. U.S.A.* **116**, 13293-13298 (2019).
22. N. V. Grishin, KH domain: one motif, two folds. *Nucleic Acids Res.* **29**, 638-643 (2001).
23. D. Hollingworth *et al.*, KH domains with impaired nucleic acid binding as a tool for functional analysis. *Nucleic Acids Res.* **40**, 6873-6886 (2012).
24. T. Talwar *et al.*, The DEAD-box protein DDX43 (HAGE) is a dual RNA-DNA helicase and has a K-homology domain required for full nucleic acid unwinding activity. *J. Biol. Chem.* **292**, 10429-10443 (2017).
25. M. Yadav *et al.*, The KH domain facilitates the substrate specificity and unwinding processivity of DDX43 helicase. *J. Biol. Chem.* **296**, 100085 (2021).
26. C. L. Lin, Y. T. Wang, W. Z. Yang, Y. Y. Hsiao, H. S. Yuan, Crystal structure of human polynucleotide phosphorylase: insights into its domain function in RNA binding and degradation. *Nucleic Acids Res.* **40**, 4146-4157 (2012).
27. Y. Zhang *et al.*, PARP9-DTX3L ubiquitin ligase targets host histone H2BJ and viral 3C protease to enhance interferon signaling and control viral infection. *Nat. Immunol.* **16**, 1215-1227 (2015).
28. A. S. Bader, B. R. Hawley, A. Wilczynska, M. Bushell, The roles of RNA in DNA double-strand break repair. *Br. J. Cancer* **122**, 613-623 (2020).
29. J. Huang *et al.*, DTX3L Enhances Type I Interferon Antiviral Response by Promoting the Ubiquitination and Phosphorylation of TBK1. *J. Virol.* **97**, e0068723 (2023).
30. M. Gabrielsen *et al.*, A General Strategy for Discovery of Inhibitors and Activators of RING and U-box E3 Ligases with Ubiquitin Variants. *Mol. Cell* **68**, 456-470.e410 (2017).
31. H. Dou, L. Buetow, G. J. Sibbet, K. Cameron, D. T. Huang, BIRC7–E2 ubiquitin conjugate structure reveals the mechanism of ubiquitin transfer by a RING dimer. *Nat. Struct. Mol. Biol.* **19**, 876-883 (2012).
32. H. Dou, L. Buetow, A. Hock, G. J. Sibbet, K. H. Vousden, D. T. Huang, Structural basis for autoinhibition and phosphorylation-dependent activation of c-Cbl. *Nat. Struct. Mol. Biol.* **19**, 184-192 (2012).
33. S. Volk, M. Wang, C. M. Pickart, Chemical and genetic strategies for manipulating polyubiquitin chain structure. *Methods Enzymol.* **399**, 3-20 (2005).
34. M. Renatus *et al.*, Structural Basis of Ubiquitin Recognition by the Deubiquitinating Protease USP2. *Structure* **14**, 1293-1302 (2006).
35. H. M. Magnussen *et al.*, Structural basis for DNA damage-induced phosphoregulation of MDM2 RING domain. *Nat. Commun.* **11**, 2094 (2020).
36. S. P. Skinner, R. H. Fogh, W. Boucher, T. J. Ragan, L. G. Mureddu, G. W. Vuister, CcpNmr AnalysisAssign: a flexible platform for integrated NMR analysis. *J. Biomol. NMR* **66**, 111-124 (2016).

Acknowledgements: We thank Core Services and Advanced Technologies at the Cancer Research UK Scotland Institute (C596/A17196 and A31287) with particular thanks to Molecular Technology services; Catherine Winchester for her assistance in critically reviewing this manuscript. **Funding:** This work was supported by Cancer research UK core grants to D.T.H. (A23278) and M.B. (A29252).

Author contributions: E.L.D., C.C., L.B., S.F.A., and D.T.H. generated constructs and purified proteins. E.L.D. and C.C. carried out the investigation. E.L.D. and B.O.S. performed NMR and analysed the data. C.C. and T.S. performed ssRNA and ssDNA binding assays and analysed with M.B. E.L.D. and D.T.H. wrote the manuscript. All authors commented on the manuscript. **Competing interests:** D.T.H is a consultant for Triana Biomedicines. The other authors declare no competing interests.

Data and materials availability: Original and uncropped images are presented in Supplemental Figures 4 and 5. Materials are available from the corresponding author (D.T.H.) upon request.

609 **Table 1. List of nucleotide sequences used in this study**

Name	Type	Sequence	Modifications
D1	ssDNA	5' TGTTTGTTTGTTTGTTTGTT 3'	5' FAM
D2	ssDNA	5' GCGCGCGCGCGCGCGCGCGC 3'	5' FAM
D3	ssDNA	5' AGTGAGTGAGTGAGTGAGTG 3'	5' FAM
D4	ssDNA	5' CAACAACAACAACAACAACA 3'	5' FAM
D5	ssDNA	5' AGAGAGAGAGAGAGAGAGAG 3'	5' FAM
D6	ssDNA	5' TCTCTCTCTCTCTCTCTCTC 3'	5' FAM
D7	ssDNA	5' TTTTTTTTTTTTTTTTTTTT 3'	5' FAM
D8	ssDNA	5' GTGCTGCGCTGCGCTGTGCT 3'	5' FAM
D9	ssDNA	5' AAAAAAAAAAAAAAAAAAAA 3'	5' FAM
D10	ssDNA	5' CAACAACAACAACAACAACA 3'	5' IRDye® 800
D11	ssDNA	5' CAACAACAACAACAACAACA 3'	None
D12	dsDNA	5' CAACAACAACAACAACAACA 3' + 3' TGTTGTTGTTGTTGTTGTTG 5'	5' FAM None
D13	ssDNA	5' CAACAACAACAACAACAACA 3'	3' FAM
D14	ssDNA	5' CAACAACAACAACAACAACA 3'	5' IRD800 3' 2FA
D15	ssDNA	5' CAACAACAACAACAACAACA 3'	5' IRDye® 800 3' Phos
D16	ssDNA	5' CAACAACAACAACAACAACT 3'	5' FAM
D17	ssDNA	5' CAACAACAACAACAACAACG 3'	5' FAM
D18	ssDNA	5' CAACAACAACAACAACAACC 3'	5' FAM
D19	ssDNA	5' CAACAACAACAACAACAAAA 3'	5' FAM
D20	ssDNA	5' CAACAACAACAACAACAATA 3'	5' FAM
D21	ssDNA	5' CAACAACAACAACAACAAGA 3'	5' FAM
D22	ssDNA	5' CAACA 3'	5' FAM
D23	ssDNA	5' AACAACAACA 3'	5' FAM
D24	ssDNA	5' AACAACAACAACAACAACAACAACAACAACAACAAC AACA 3'	5' FAM
D25	ssDNA	5' CAACAACAACAACAACAACAACAACAACAACAACAA CAACAACAACAACAACAACAACAACAACAACAACAA CAACAACA 3'	5' FAM
D26	ssDNA	CGGCACATCACTCTTCAACA	5' FAM
D27	dsDNA	5' CGGCACATCACTCTTCAACA 3' + 5' GTTGAAGAGTGATGTGCCG 3'	5' FAM None
D28	dsDNA	5' CGGCACATCACTCTTCAACA 3' + 5' TTGAAGAGTGATGTGCCG 3'	5' FAM None
D29	dsDNA	5' CGGCACATCACTCTTCAACA 3' + 5' TGAAGAGTGATGTGCCG 3'	5' FAM None
D30	ssDNA	CAACA	None
D31	ssDNA	5' CAACAACAACAACAACAACA 3'	3' Phos
R1	ssRNA	5' UGUUUGUUUGUUUGUUUGUU 3'	5' FAM
R2	ssRNA	5' GCGCGCGCGCGCGCGCGCGC 3'	5' FAM
R3	ssRNA	5' AGUGAGUGAGUGAGUGAGUG 3'	5' FAM
R4	ssRNA	5' CAACAACAACAACAACAACA 3'	5' FAM
R5	ssRNA	5' AGAGAGAGAGAGAGAGAGAG 3'	5' FAM
R6	ssRNA	5' UCUCUCUCUCUCUCUCUCUC 3'	5' FAM
R7	ssRNA	5' UUUUUUUUUUUUUUUUUUUU 3'	5' FAM
R8	ssRNA	5' GUGCUGCGCUGCGCUGUGCU 3'	5' FAM
R9	ssRNA	5' AAAAAAAAAAAAAAAAAAAA 3'	5' FAM

610

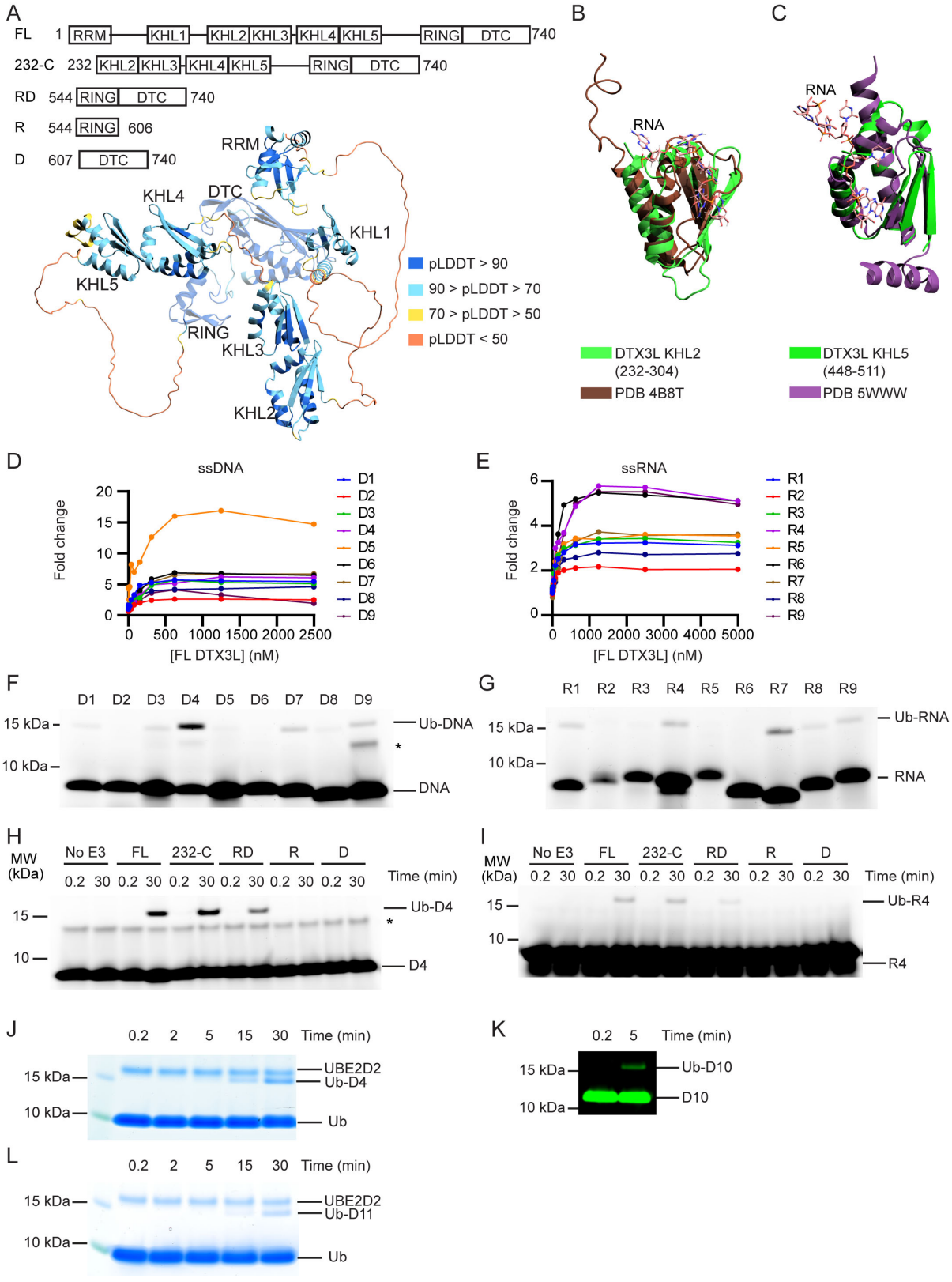

Figure 1. DTX3L catalyses ubiquitination of single-stranded nucleic acids.

(A) Cartoon representation of the AlphaFold model of DTX3L. Domains are coloured according to model confidence. Domain architecture of DTX3L constructs is shown above the model. **(B)** DTX3L

615 KHL2 (232-304) prediction shown in green overlaid with the third KH domain of KSRP in complex
616 with AGGGU RNA sequence (PDB 4B8T) shown in brown. **(C)** DTX3L KHL5 (448-511) prediction
617 shown in green overlaid with the MEX-3C KH1 domain in complex with GUUUAG RNA sequence
618 (PDB 5WWW) shown in purple. **(D)** Fold change of fluorescence polarisation of 6-FAM-labelled
619 ssDNA D1-9 upon titrating with full-length DTX3L. **(E)** As in (D) but with 6-FAM-labelled ssRNA
620 R1-9. **(F)** Fluorescently detected SDS-PAGE gel of *in vitro* ubiquitination of 6-FAM-labelled ssDNA
621 D1-9 oligonucleotides by FL DTX3L in the presence of E1, UBE2D2, Ub, Mg^{2+}-ATP. **(G)** As in (F) but
622 with 6-FAM-labelled ssRNA R1-9 oligonucleotides. **(H)** Fluorescently detected SDS-PAGE gel of *in*
623 *vitro* ubiquitination of 6-FAM-labelled ssDNA D4 by DTX3L variants (FL, full length; RD, RING-
624 DTC domains; R, RING domain; D, DTC domain) in the presence of E1, UBE2D2, Ub, Mg^{2+}-ATP. **(I)**
625 As in (H) but with 6-FAM-labelled ssRNA R4. **(J)** Coomassie stained SDS-PAGE gel of *in vitro*
626 ubiquitination of 6-FAM-labelled ssDNA D4 by DTX3L-RD in the presence of E1, UBE2D2, Ub,
627 Mg^{2+}-ATP. (**K**) Fluorescently detected SDS-PAGE gel of *in vitro* ubiquitination of 5' IRDye® 800
628 ssDNA D10 by DTX3L-RD in the presence of E1, UBE2D2, Ub, Mg^{2+}-ATP. (**L**) Coomassie stained
629 SDS-PAGE gel of *in vitro* ubiquitination of ssDNA D11 by DTX3L-RD in the presence of E1, UBE2D2,
630 Ub, Mg^{2+}-ATP. Asterisks in (F) and (H) indicate contaminant bands from ssDNA or ssRNA. Uncropped
631 gel images for (F–L) are shown in fig. S4.

632

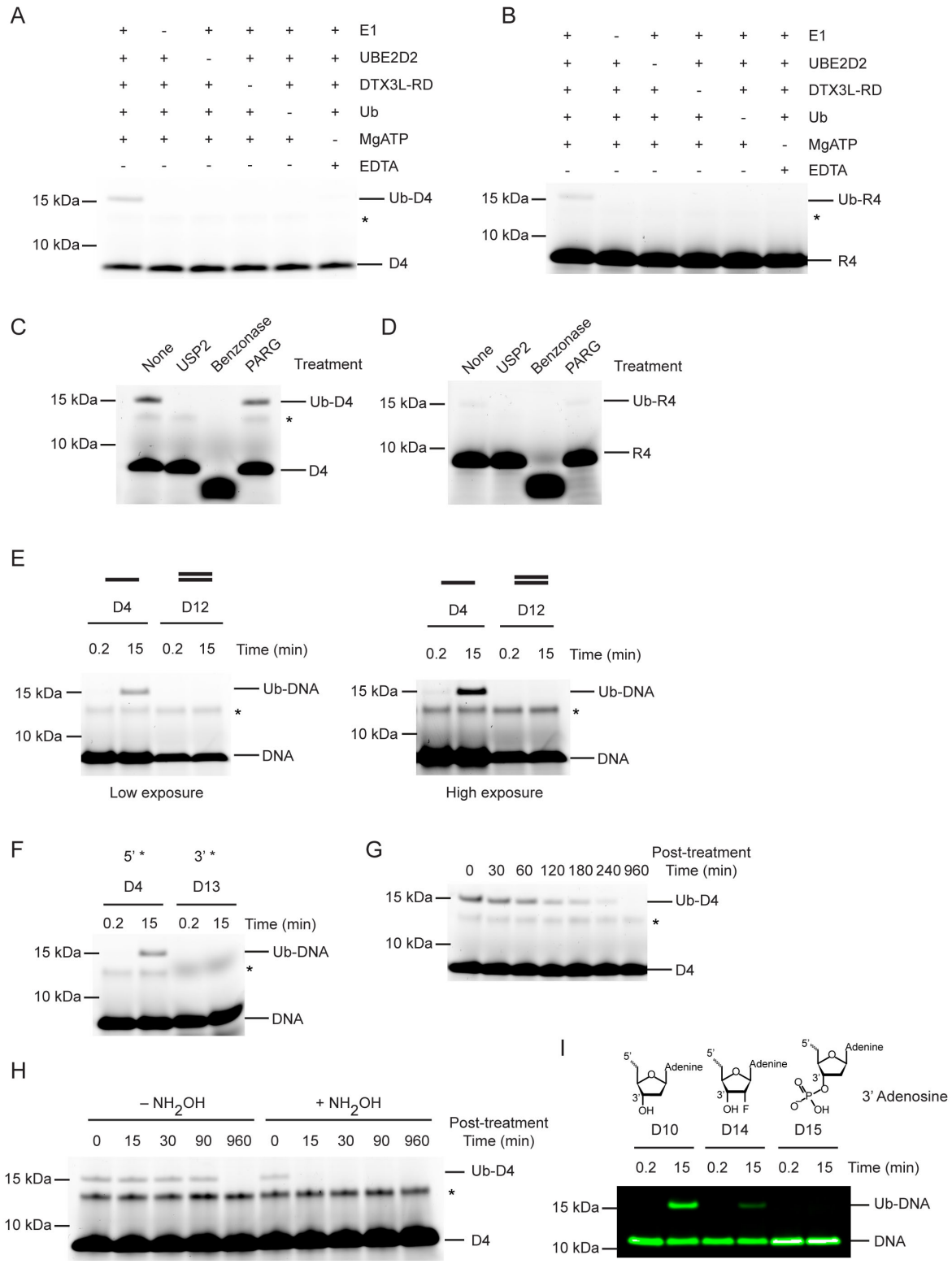

Figure 2. Ub modification of ssDNA occurs at the 3' hydroxyl at the 3' end.

(A) Fluorescently detected SDS-PAGE gel of *in vitro* ubiquitination of ssDNA D4 in which E1, UBE2D2, DTX3L-RD, Ub or Mg^{2+}-ATP have been omitted. **(B)** As in (A) but with 6-FAM-labelled

637 ssRNA R4. **(C)** Fluorescently detected SDS-PAGE gel of i*n vitro* ubiquitination of 6-FAM-labelled
638 ssDNA D4 by DTX3L-RD in the presence of E1, UBE2D2, Ub, Mg^{2+}-ATP subsequently treated with
639 USP2, Benzonase, PARG or not treated (None). **(D)** As in (C) but with 6-FAM-labelled ssRNA R4. **(E)**
640 Fluorescently detected SDS-PAGE gel of *in vitro* ubiquitination of 6-FAM-labelled ssDNA D4 and
641 dsDNA D12 oligonucleotides by DTX3L-RD (left panel) and at increased exposure (right panel) in the
642 presence of E1, UBE2D2, Ub, Mg^{2+}-ATP. **(F)** As in (E) but with 6-FAM-labelled ssDNA D4 (5' label)
643 and D13 (3' label) oligonucleotides. **(G)** Fluorescently detected SDS-PAGE gel of *in vitro* ubiquitinated
644 of 6-FAM-labelled ssDNA D4 subsequently treated with pH 9.5 buffer for the times indicated. **(H)**
645 Fluorescently detected SDS-PAGE gel of *in vitro* ubiquitinated of 6-FAM-labelled ssDNA D4
646 subsequently treated with 1.5 M NH_2OH at pH 9 for the times indicated. **(I)** As in (E) but with 5'
647 IRDye® 800 ssDNA D10, D14 and D15 oligonucleotides. Asterisks in (A–C) and (E–H) indicate
648 contaminant band from ssDNA or ssRNA. Uncropped gel images are shown in fig. S4.

649

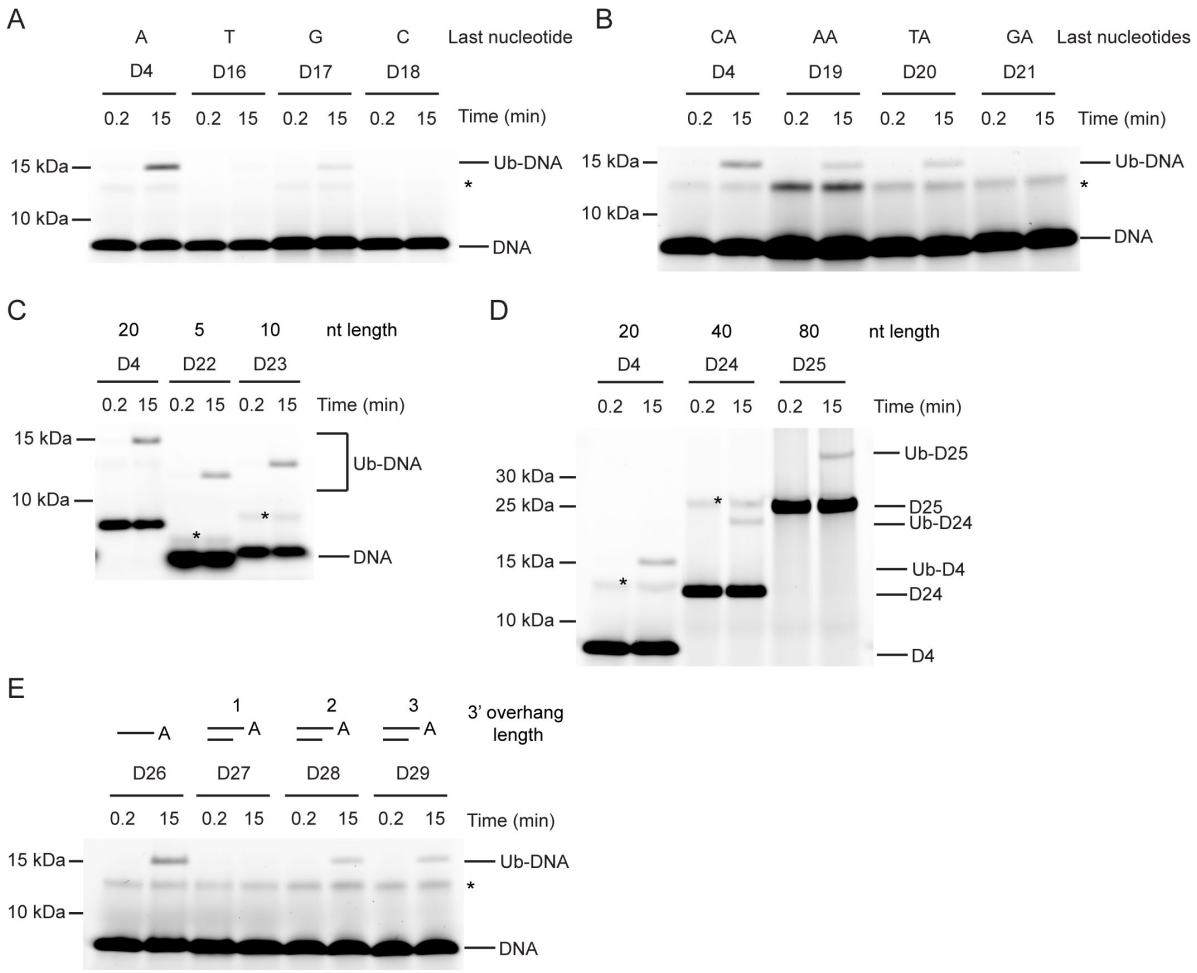

Figure 3. Nucleotide sequence requirements for Ub-DNA formation.

Fluorescently detected SDS-PAGE gel of *in vitro* ubiquitination (in the presence of E1, UBE2D2, Ub, and Mg^{2+}-ATP) of **(A)** 6-FAM-labelled ssDNA D4, D16, D17 and D18 by DTX3L-RD. **(B)** 6-FAM-labelled ssDNA D4, D19, D20 and D21 by DTX3L-RD. **(C)** 6-FAM-labelled ssDNA D4, D22 and D23 by DTX3L-RD. **(D)** 6-FAM-labelled ssDNA D4, D24 and D25 by DTX3L-RD. **(E)** 6-FAM-labelled ssDNA D26, dsDNA D27, D28 and D29 by DTX3L-RD. Asterisks indicate contaminant band from ssDNA. Uncropped gel images are shown in fig. S4.

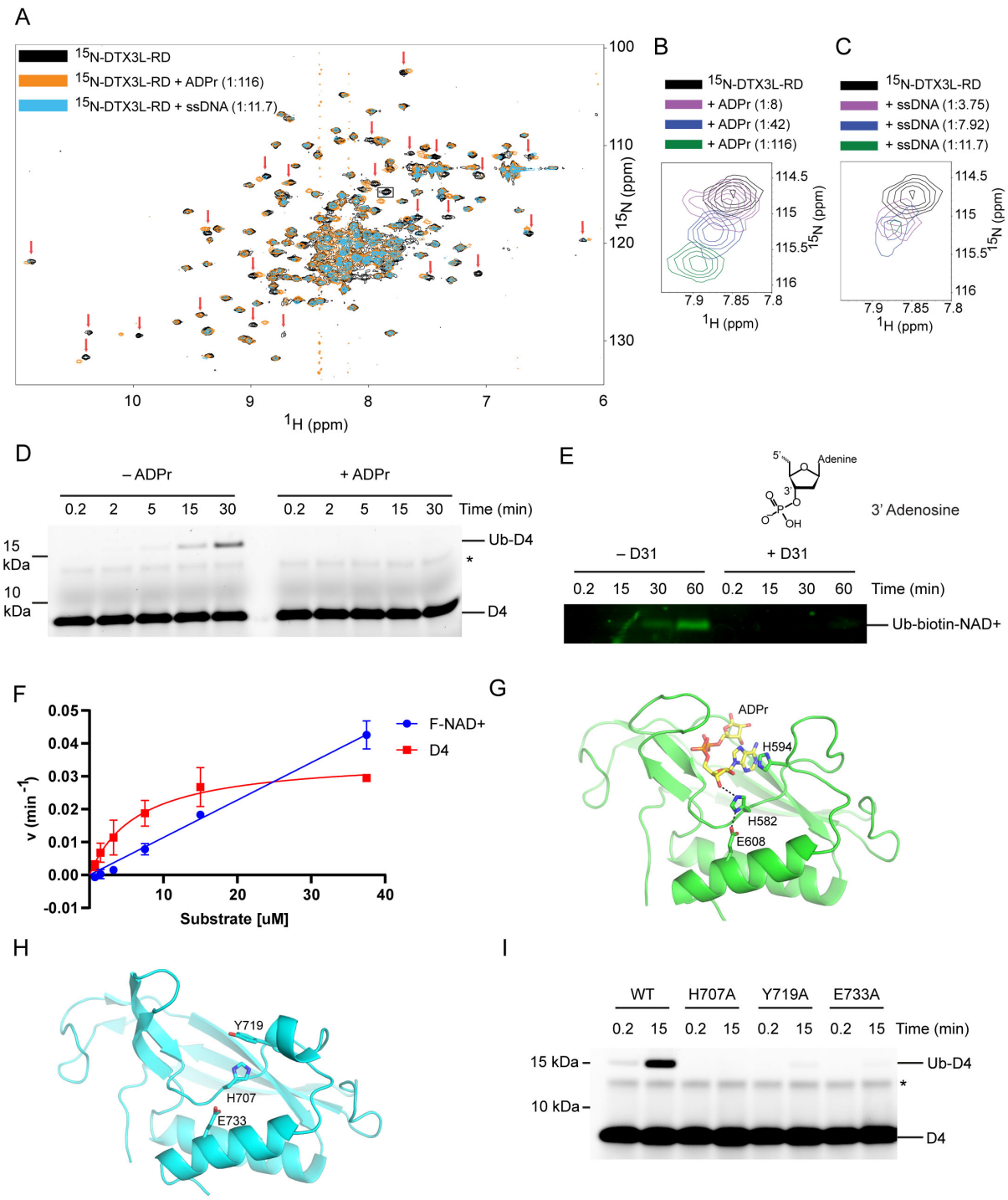

Figure 4. DTX3L DTC domain binds and facilitates Ub-DNA formation.

(A) ^{1}H-^{15}N HSQC spectra of ^{15}N-DTX3L-RD (black), ADPr-^{15}N-DTX3L-RD (orange), and ssDNA D30-^{15}N-DTX3L-RD (blue). Red arrows indicate cross peaks that shift upon titrating with ADPr or ssDNA. **(B)** Close-up view of the cross peak indicated by black box in (A) upon titration of specified molar ratios of ADPr with ^{15}N-DTX3L-RD. **(C)** Close-up view of the cross peak indicated by black

665 arrow in (A) upon titration of specified molar ratios of ssDNA D30 with ^{15}N-DTX3L-RD. **(D)**
666 Fluorescently detected SDS-PAGE gel of *in vitro* ubiquitination of 6-FAM-labelled ssDNA D4 by
667 DTX3L-RD in the presence of E1, UBE2D2, Ub, Mg^{2+}-ATP and treated with excess ADPr. **(E)** Western
668 Blot of *in vitro* ubiquitination of biotin-NAD^+ by DTX3L-RD in the presence of E1, UBE2D2, Ub,
669 Mg^{2+}-ATP and treated with excess ssDNA D31. **(F)** Kinetics of Ub-D4 and Ub-F-NAD^+ formation
670 catalysed by DTX3L-RD. Data from two independent experiments (n=2) were fitted with the
671 Michaelis–Menten equation and k_{cat}/K_m value for D4 (5457 M^{-1} min^{-1}) calculated. k_{cat}/K_m value for F-
672 NAD^+ (1190 M^{-1} min^{-1}) was estimated from the slope of the linear portion of curve. **(G)** Structure of
673 DTX2-DTC domain (green) bound to ADPr (yellow) (PDB: 6Y3J). The sidechains of H582, H594 and
674 E608 are shown in sticks. Hydrogen bonds are indicated by dotted lines. **(H)** Structure of DTX3L-DTC
675 domain (cyan; PDB: 3PG6). The sidechains of H707, Y719 and E733 are shown in sticks. **(I)**
676 Fluorescently detected SDS-PAGE gel of *in vitro* ubiquitination of 6-FAM-labelled ssDNA D4 by full
677 length DTX3L WT, H707A, Y719A and E733A in the presence of E1, UBE2D2, Ub, Mg^{2+}-ATP.
678 Asterisks in (D) and (I) indicate contaminant band from ssDNA. Uncropped gel images of (D), (E) and
679 (I) are shown in fig. S5.

680

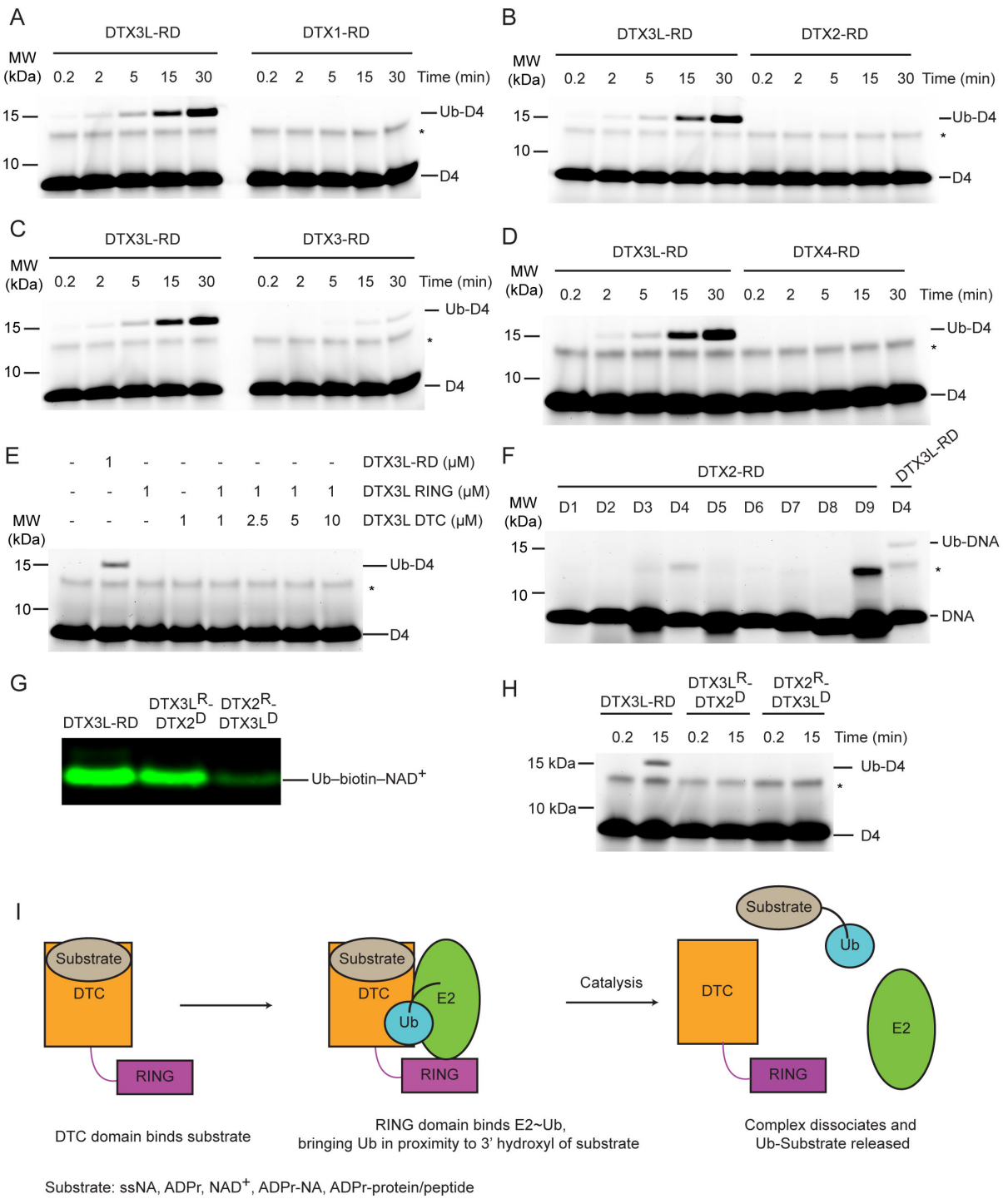

Figure 5. Select DTX RING-DTC domains catalyse ubiquitination of ssDNA.

(A) Fluorescently detected SDS-PAGE gel of *in vitro* ubiquitination of 6-FAM-labelled ssDNA D4 by DTX3L-RD or DTX1-RD in the presence of E1, UBE2D2, Ub, Mg^{2+}-ATP. **(B)** As in (A) but with DTX2-RD. **(C)** As in (A) but with DTX3-RD. **(D)** As in (A) but with DTX4-RD. **(E)** As in (A) but with DTX3L-RD or DTX3L RING with increasing concentrations of DTX3L DTC. **(F)** Fluorescently

687 detected SDS-PAGE gel of *in vitro* ubiquitination of 6-FAM-labelled ssDNA D1-9 by DTX2-RD. A
688 reaction with DTX3L-RD and 6-FAM-labelled ssDNA D4 was included as a positive control. **(G)**
689 Western blot of *in vitro* ubiquitination of biotin-NAD^+ in the presence of E1, UBE2D2, Ub, Mg^{2+}-ATP,
690 NAD^+, biotin-NAD^+ with either DTX3L-RD, $DTX3L^R$-$DTX2^D$, or $DTX2^R$-$DTX3L^D$ and separated by
691 SDS-PAGE. **(H)** Fluorescently detected SDS-PAGE gel of *in vitro* ubiquitination of 6-FAM-labelled
692 ssDNA D4 by DTX3L-RD, $DTX3L^R$-$DTX2^D$, or $DTX2^R$-$DTX3L^D$ in the presence of E1, UBE2D2, Ub,
693 Mg^{2+}-ATP. **(I)** Schematic diagrams showing the proposed mechanism of ubiquitination of substrates by
694 DTX3L-RD. Asterisks in (A–F) and (H) indicate contaminant band from ssDNA. Uncropped gel images
695 of (A–H) are shown in fig. S5.

696

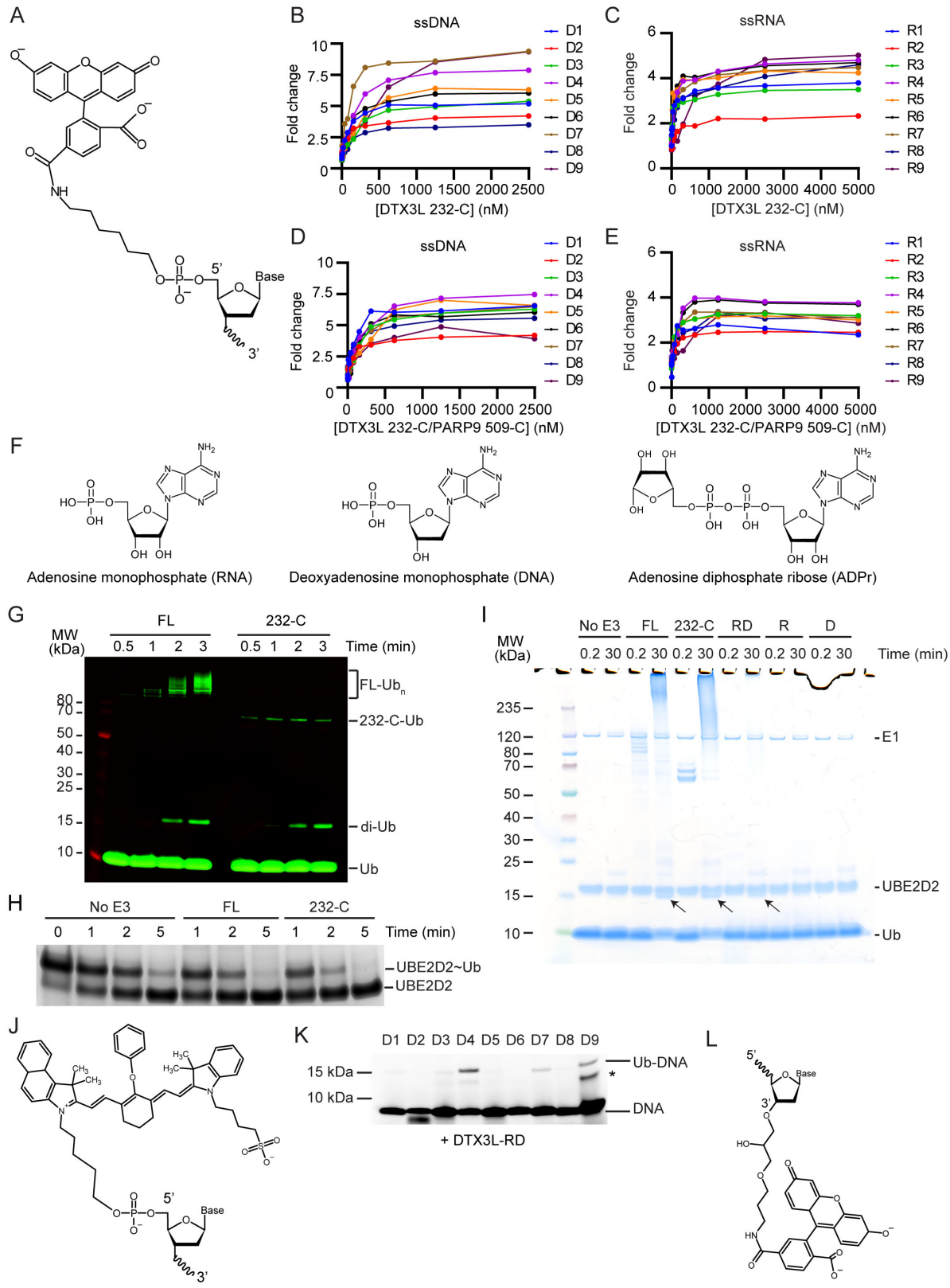

Figure S1. DTX3L binds and ubiquitinates ssNAs.

699 **(A)** Schematic of the 5' 6-FAM modification. **(B)** Fold change of fluorescence polarisation of 6-FAM-
700 labelled ssDNA D1-9 oligonucleotides upon titrating with DTX3L 232-C. **(C)** As in (B) but with 6-
701 FAM-labelled ssRNA R1-9 oligonucleotides. **(D)** As in (B) but with DTX3L 232-C/PARP9 509-C. **(E)**
702 As in (D) but with 6-FAM-labelled ssRNA R1-9. **(F)** Schematic of RNA, DNA and ADPr. **(G)**
703 Fluorescently detected SDS-PAGE gel of *in vitro* autoubiquitination of DTX3L FL and 232-C in the
704 presence of E1, UBE2D2, fluorescent-labelled Ub and Mg^{2+}-ATP. **(H)** Coomassie stained SDS-PAGE
705 gel of lysine discharge reactions showing disappearance of UBE2D2~Ub over time in the presence of
706 FL, 232-C or absence of E3. **(I)** Coomassie stained SDS-PAGE gel of *in vitro* ubiquitination of 6-FAM-
707 labelled ssDNA D4 by DTX3L variants in the presence of E1, UBE2D2, Ub, Mg^{2+}-ATP (from Fig. 1H).
708 Arrows indicate potential ~15 kDa Ub-DNA band. **(J)** Schematic of IRDye® 800 modification. **(K)**
709 Fluorescently detected SDS-PAGE gel of *in vitro* ubiquitination of 6-FAM-labelled ssDNA D1-9 in the
710 presence of E1, UBE2D2, Ub, Mg^{2+}-ATP by DTX3L-RD. **(L)** Schematic of the 3' 6-FAM modification.
711 Asterisks in (K) indicate contaminant band from ssDNA. Uncropped gel images of (H) and (K) are
712 shown in fig. S5.

713

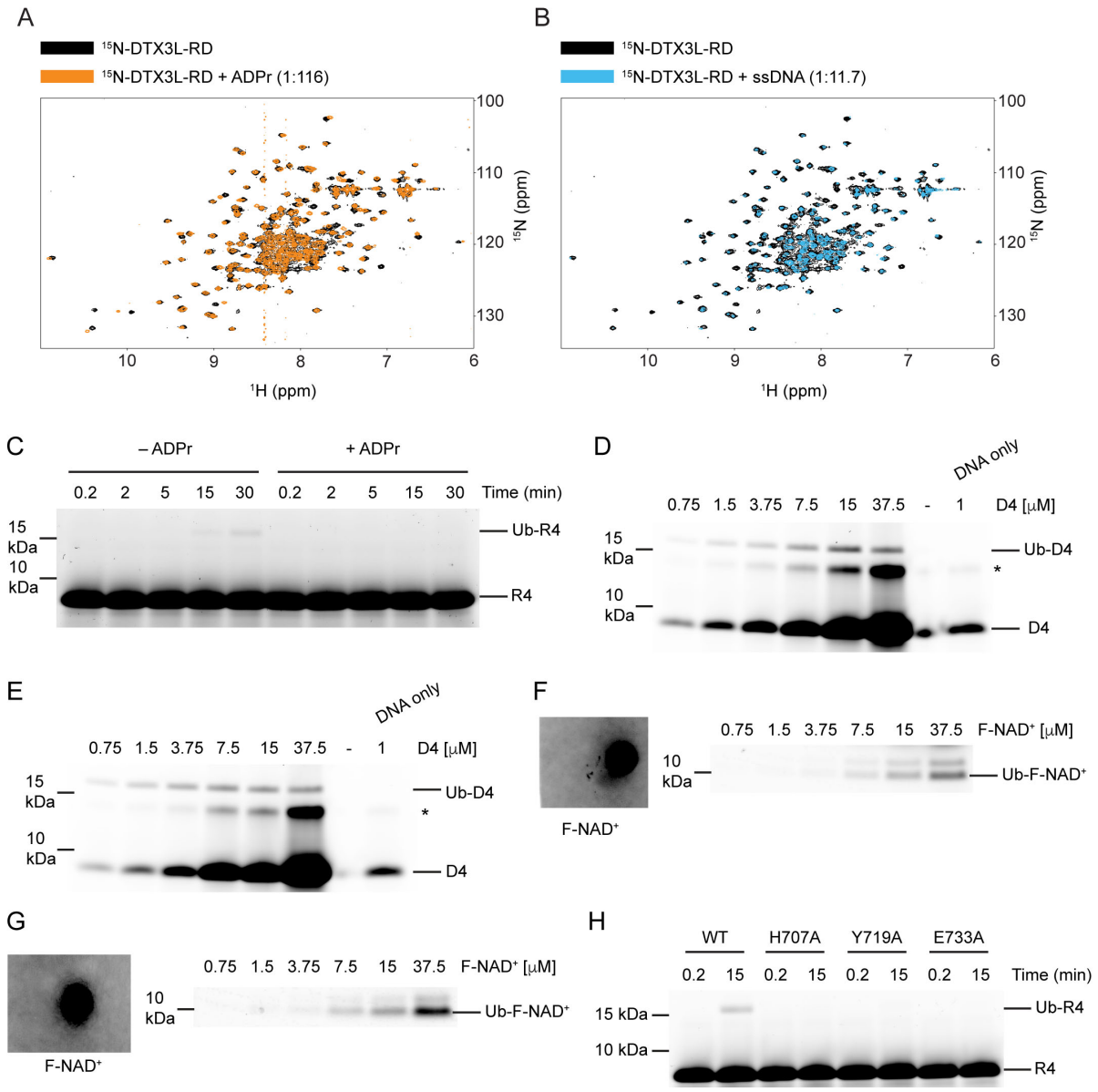

Figure S2. DTX3L-RD binds ADPr and ssNA.

(A) ^{1}H-^{15}N HSQC spectra of ^{15}N-DTX3L-RD (black) and after the addition of ADPr (orange) (related to Fig. 4A). **(B)** ^{1}H-^{15}N HSQC spectra of ^{15}N-DTX3L-RD (black) and after the addition of ssDNA D30 (blue) (related to Fig. 4A). **(C)** Fluorescently detected SDS-PAGE gel of *in vitro* ubiquitination of 6-FAM-labelled ssRNA R4 by DTX3L-RD in the presence of E1, UBE2D2, Ub, Mg^{2+}-ATP and treated with excess ADPr. **(D)** Fluorescently detected SDS-PAGE gel of *in vitro* ubiquitination of increasing concentrations of 6-FAM-labelled ssDNA D4 by DTX3L-RD in the presence of E1, UBE2D2, Ub, Mg^{2+}-ATP. **(E)** Replicate of (D). **(F)** Fluorescently detected SDS-PAGE gel of *in vitro* ubiquitination of increasing concentrations of F-NAD^{+} by DTX3L-RD in the presence of E1, UBE2D2, Ub, Mg^{2+}-ATP.

724 A known volume of 100 μM F-NAD^+ was pipetted onto Whatman filter paper and scanned alongside
725 the gel for quantification. **(G)** Replicate of (F). **(H)** Fluorescently detected SDS-PAGE gel of *in vitro*
726 ubiquitination of 6-FAM-labelled ssRNA R4 by FL DTX3L WT, H707A, Y719A and E733A in the
727 presence of E1, UBE2D2, Ub, Mg^{2+}-ATP. Asterisks in (D) and (E) indicate contaminant band from
728 ssDNA. Uncropped gel images of (C-H) are shown in fig. S5.

729

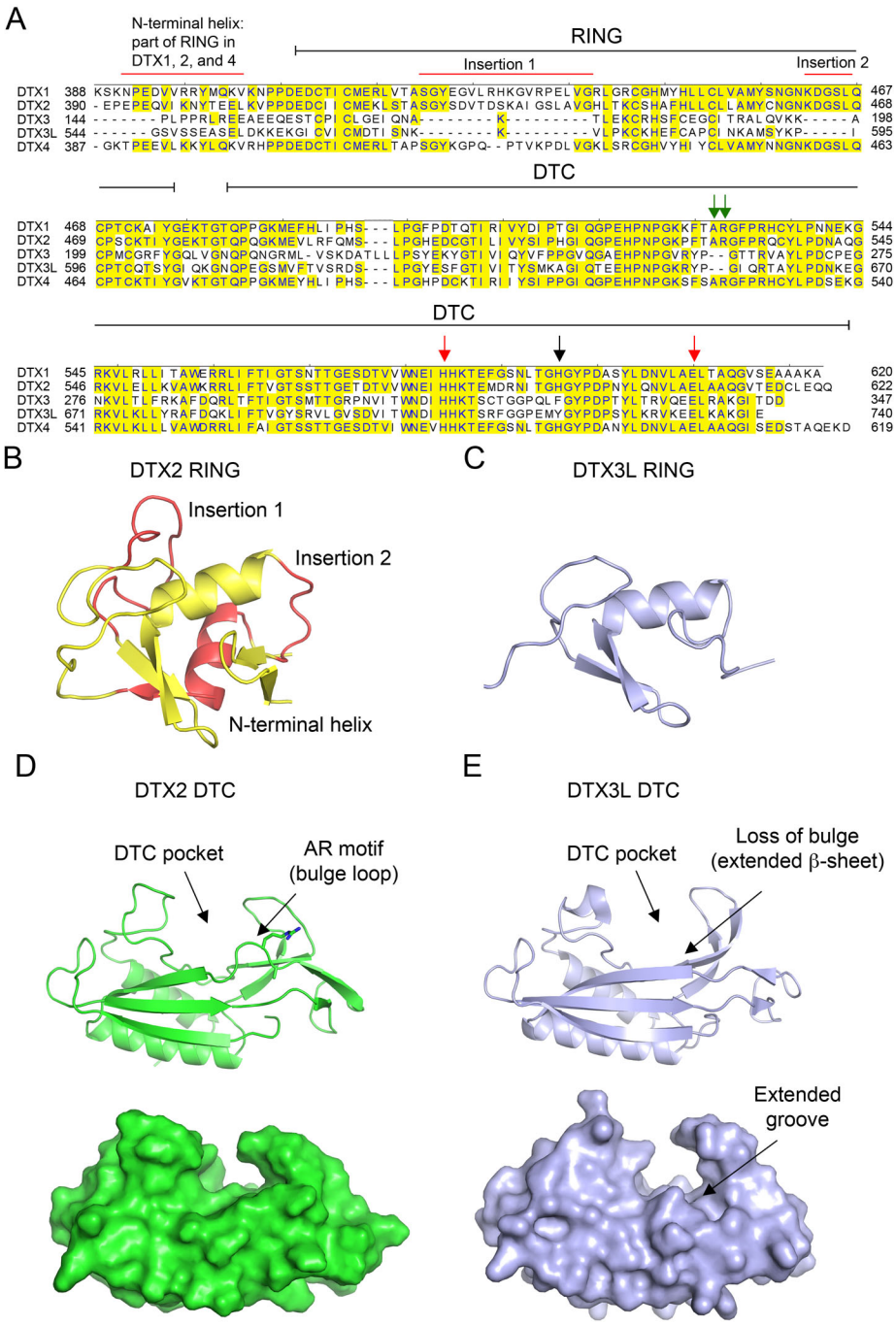

Figure S3. Properties of DTX family DTC domains.

(**A**) Sequence alignment of human DTX family RING-DTC domains. Starting and ending residues of RING-DTC domains are indicated. Conserved residues are highlighted in yellow. A black arrow indicates residue that stacks with ADPr, red arrows indicate conserved catalytic residues, and green arrows indicate AR motif present in DTX1, 2, and 4. Insertions are indicated. (**B**) Structure of DTX2 RING domain (from PDB: 6Y3J). The insertions and N-terminal helix are colored in red and the

conserved RING domain region is colored yellow. (**C**) Alphafold2 model of DTX3L RING domain (light blue) displayed in the same orientation as in B. (**D**) Top: cartoon representation of structure of DTX2 DTC domain (green; PDB: 6Y3J). Sidechains of AR motif are shown as sticks. The DTC pocket that binds ADPr and the bulged AR motif are indicated by arrows. Bottom: as in top panel but with surface representation. (**E**) Top: cartoon representation of structure of DTX3L DTC domain (light blue; PDB: 3PG6). Bottom: as in top panel but with surface representation. The absence of an AR motif in DTX3L causes a slight structural change near the ADPr-binding pocket, leading to the loss of the bulged loop, which results in a slightly extended groove.

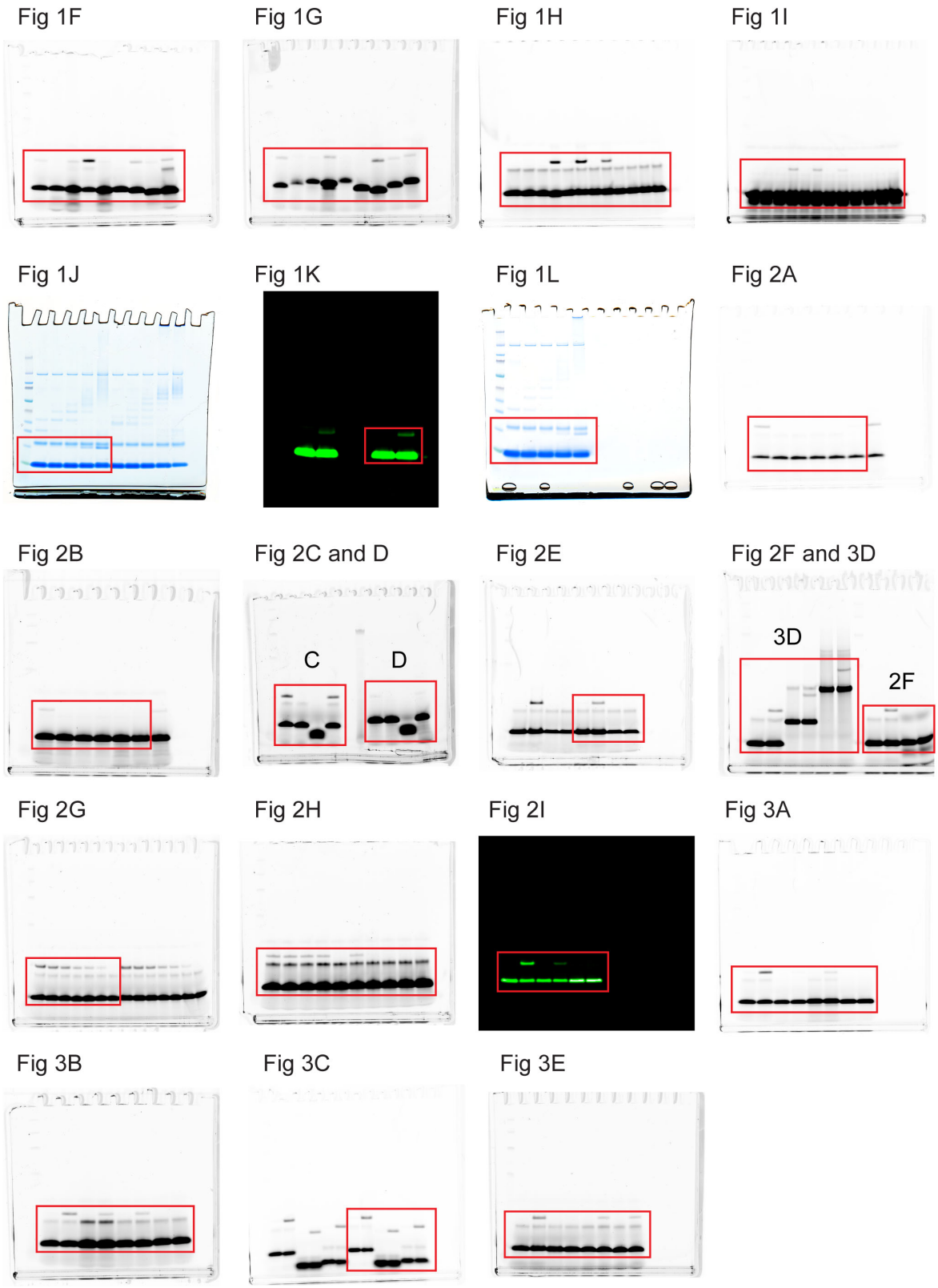

Figure S4

Full images of gels from Figure 1-3. Red boxes denote where images were cropped.

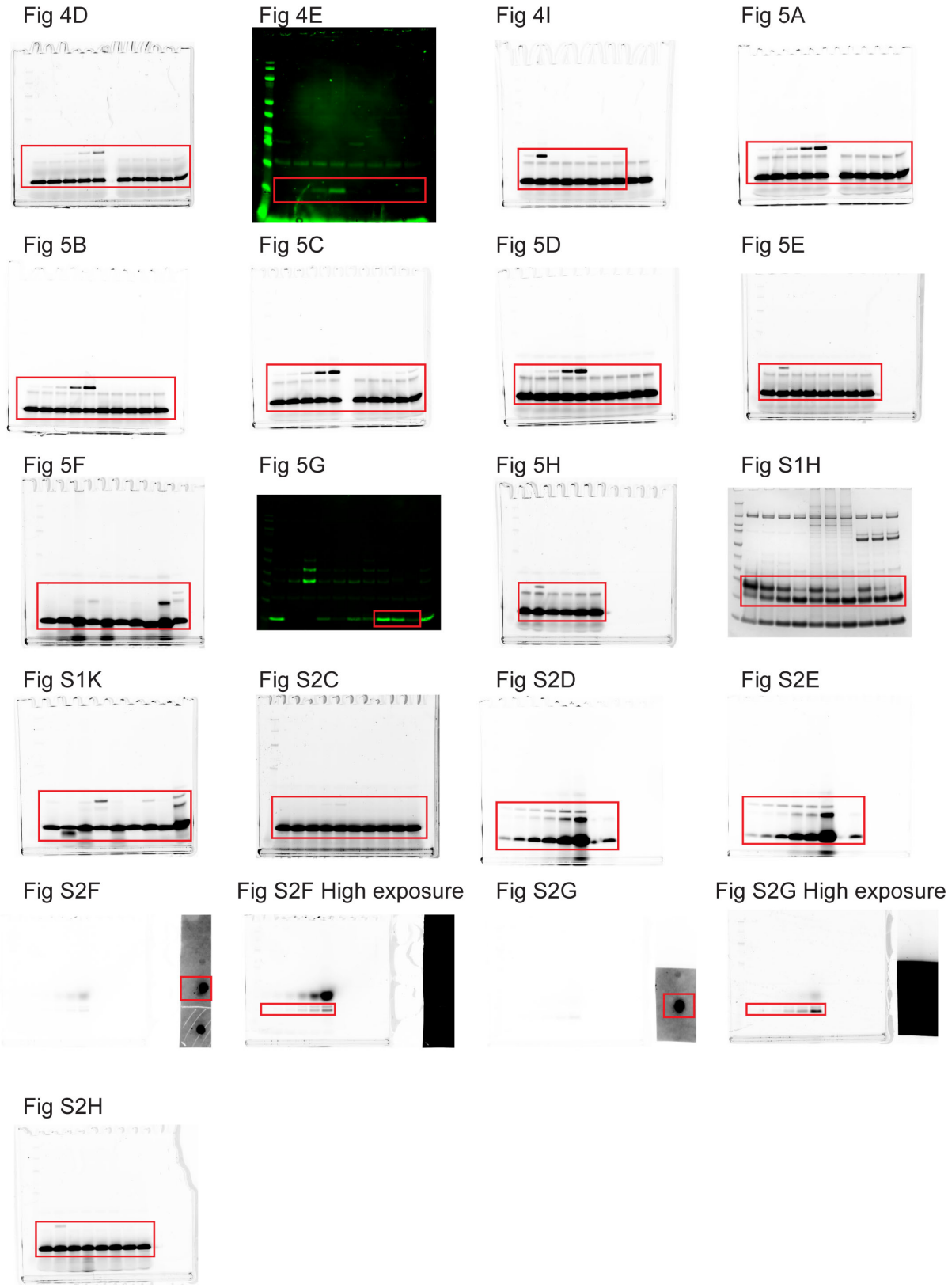

Figure S5

Full images of gels from Figure 4-5 and S1-2. Red boxes denote where images were cropped.